

UNIVERSITY OF CALIFORNIA
Los Angeles

**Augmentation of Human Upper-Limb Motion
and Physical Human-Exoskeleton Interaction**

A prospectus submitted in partial satisfaction
of the requirements for the degree
Doctor of Philosophy in Mechanical Engineering

by

Guanyu Chen

2025

© Copyright by
Guanyu Chen
2025

The prospectus of Guanyu Chen is approved.

Tsu-Chin Tsao

Veronica Santos

Dennis Hong

Jacob Rosen, Committee Chair

University of California, Los Angeles

2025

TABLE OF CONTENTS

1	Introduction	1
1.1	Background	1
1.2	EXO-UL8	2
1.3	Outline	4
2	Upper-Limb Neurological Impairment Rehabilitation Based On Self-Interactive Assist-As-Needed Algorithm	6
2.1	Introduction	6
2.2	Literature Review	7
2.3	Research Question	11
2.4	Self-Interactive Characteristic	11
2.5	Reference Trajectory Generation	12
2.6	General Model	14
2.6.1	Assumptions	14
2.6.2	Cross-Section Shape of the Virtual Tunnels	14
2.6.3	Arm Kinematics	14
2.6.4	Properties of Self-Interactive Characteristic	16
2.6.5	Case Study	19
2.7	Virtual Tunnel Creation	20
2.8	Validation of Self-Interactive Characteristic	21
2.9	Validation of Virtual Tunnel Creation	23
2.10	Research Plan	24
3	Upper-limb Redundancy Resolution	27
3.1	Introduction	27
3.2	Literature Review	28
3.2.1	Redundancy Resolution	28
3.2.2	Synergistic Motion	30
3.3	Research Question	33
3.4	Research Plan	34
3.4.1	Method	34

3.4.2	Data Collection	34
3.4.3	Processing	34
4	Augmentation of Physical Human-Exoskeleton Interaction Transparency	36
4.1	Introduction	36
4.2	Literature Review	37
4.2.1	Transparency Improvement	37
4.2.2	Measures of Transparency	41
4.3	Research Question	43
4.4	Research Plan	43
5	Conclusion	46
References		47
A	Gantt Chart	61

LIST OF FIGURES

1.1 EXO-UL8: A dual-arm powered upper-limb exoskeleton.	3
1.2 Control Scheme of EXO-UL8.	3
2.1 Bicycle cranking model [20].	8
2.2 Force field generated (a) band paradigm (b) window paradigm [21].	8
2.3 Iterative learning controller [22].	9
2.4 Adaptive control based on Gaussian RBFs with a forgetting term (force decay) [28]. The desired state, generated by the designed games, is compared with the current state to produce an error signal. One branch of this error signal is fed into a PD feedback controller, while the other is directed to an adaptive controller. The output of the adaptive controller provides an estimated minimal assistance, which is then assigned to the Gaussian RBFs at the current position. Finally, this estimated assistance is added to the output of the PD controller, and their sum forms the motor command.	10
2.5 Concept of the self-interactive characteristic. Left: both joints have normal capability. Middle: one of the joints has a reduced capability. Right: A slope is added to create a beneficial loop between the two joints.	11
2.6 The arm model (left) and virtual tunnels (right).	15
2.7 Task for shoulder and elbow flexion/extension.	21
2.8 Total interactive torque over time for slow trials. (a) Torque on the shoulder. (b) Torque on the elbow.	25
2.9 Reference and actual state of the wrist of subject 2 in one of the fast trials. (a) Trajectory of the wrist (b) Wrist position in y-axis with respect to time (c) Wrist position in z-axis with respect to time (d) Wrist speed with respect to time.	26
3.1 Arm model with shoulder adduction/abduction (θ_1), flexion/extension (θ_2), and internal/external rotations (θ_3); elbow flexion/extension (θ_4); and wrist supination/pronation (θ_5), radial/ulnar deviation (θ_6), and flexion/extension (θ_7) [57].	28
3.2 Trajectories generated by minimum-angular jerk with time adjustment [42].	29
3.3 Estimated swivel angles based on the five criteria. (a) results obtained from the least square method (b) results obtained from the exponential method [68].	31
3.4 Synergy of arm movement [75].	33
3.5 Reaching tasks [68]. (a) Top view (b) Front view (c) Task targets (d) Reflective markers on the arm.	35

4.1	Complete controller: combination of the gravity compensation feedforward and force feedback [107].	38
4.2	Interaction force on the upper arm and forearm [107].	38
4.3	Admittance control schemes used in [14]. Scheme A: hyper parameter-based. Scheme B: Kalman filter-based.	39
4.4	Admittance control based on redundancy resolution [108].	40
A.1	Gantt chart for PhD research	61

LIST OF TABLES

1.1	Anatomical and exoskeleton joint limits.	4
2.1	DH parameters of the arm model	15

CHAPTER 1

Introduction

1.1 Background

The global incidence of stroke is concerning, with over 12.2 million new cases occurring each year [1]. A stroke often leads to severe motor impairments, such as spasticity, weakness, or paralysis, which significantly hinder daily activities and diminish the quality of life [2]. Nevertheless, active, repetitive, and goal-directed training has been shown to play a crucial role in motor function recovery [3–5]. Physical therapists are integral to this recovery process, guiding patients through repetitive exercises aimed at reestablishing motor patterns [4]. However, the growing number of stroke survivors and the time-consuming nature of therapy pose significant challenges [6]. In response to these challenges, rehabilitation robots have become an important adjunct to traditional therapy methods [7, 8]. These robots provide intensive and sustained therapy that supports the recovery of motor function [9], and studies indicate that robotic rehabilitation can offer outcomes that are at least comparable, if not superior, to traditional therapy of similar intensity [10, 11].

A critical challenge in developing effective robotic rehabilitation systems is ensuring that they can emulate the complex, adaptive movements of the human arm. The human arm’s ability to achieve the same end-effector position through various joint configurations—a capability known as redundancy—is both an asset and a challenge in designing assistive devices and algorithms. Redundancy resolution with reduced number of degrees of freedom (DoF) refers to understanding how individuals adapt their movement strategies when certain joint movements are restricted or when specific joints lose functionality. This research explores the mechanisms by which the human arm compensates for such limitations, which can inform the design of more effective rehabilitation tools. The insights gained from studying human redundancy resolution have significant implications beyond rehabilitation. For instance, these principles can be applied to robotic path planning, where understanding and mimicking human strategies can lead to more efficient and human-like movements in robots. By integrating these adaptive strategies into robotic systems, we can improve their ability to perform complex tasks in dynamic environments, thereby enhancing their usefulness in both clinical and everyday settings.

The influence of synergistic motion in the arm is a crucial area of investigation. Synergy enables the nervous system to streamline the control of complex movements by organizing muscles into coordinated units. While the synergy of the hand has been studied at both the muscular and kinematic levels, research on the arm’s synergy at the kinematic level has

been relatively scarce. Previous studies have explored how external factors, such as loads, target distance, and target direction, impact these synergies. However, the effect of initial conditions has received little attention. By examining the influence of initial conditions on these synergies, we aim to optimize rehabilitation protocols and improve the design of assistive devices and therapy, ensuring they support natural movement patterns and enhance recovery outcomes.

Enhancing exoskeleton transparency is a key focus of this research. Achieving transparency—where an exoskeleton moves seamlessly with the user, without resistance or delay—is crucial for improving user experience. This enhancement not only increases the immersion and sense of freedom for users, including those beyond just patients, but also ensures that the device integrates smoothly with the user’s natural movements. By advancing the control algorithms that contribute to exoskeleton transparency, we can significantly improve the usability and effectiveness of these devices, making them more beneficial for a wider range of applications.

In summary, this dissertation investigates the complex dynamics of human arm movement, focusing on redundancy resolution and the effects of initial conditions on motor control, as well as the development of advanced rehabilitation algorithms. By integrating theoretical analysis, experimental validation, and algorithm development, this research aims to deepen the understanding of human motor control fundamentals and enhance rehabilitation strategies and advance assistive technologies, ultimately improving the quality of life for individuals with motor impairments.

1.2 EXO-UL8

The EXO-UL8 shown in Figure 1.1 is a dual-arm, powered upper-limb exoskeleton with redundant design, featuring seven active degrees of freedom (DoF) and an additional active DoF for the gripper on each arm [12–14]. This exoskeleton was developed to support research efforts in the field of robot-assisted rehabilitation. The structure of the EXO-UL8’s arms mirrors that of a healthy human’s arms, with joints that correspond closely to the anatomical joints: shoulder abduction/adduction and flexion/extension are controlled by the first two joints, shoulder internal/external rotation by the third, elbow flexion/extension by the fourth, forearm pronation/supination by the fifth, wrist flexion/extension by the sixth, and wrist radial/ulnar deviation by the seventh. Additionally, the eighth joint governs the opening and closing of the hand. All joints are revolute, ensuring consistency with their human counterparts. The range of motion for both the anatomical joints and the exoskeleton is summarized in Table 1.1, with anatomical values sourced from [15]. It is important to note that the eighth joint, responsible for hand operation, is excluded from the analysis in this chapter since it does not impact the admittance control of the EXO-UL8’s arm. To facilitate admittance control, each arm is equipped with three six-axis force/torque sensors (ATImini 40) that measure interaction forces between the operator and the exoskeleton. These sensors are strategically positioned at the upper arm, lower arm, and within the wrist assembly.

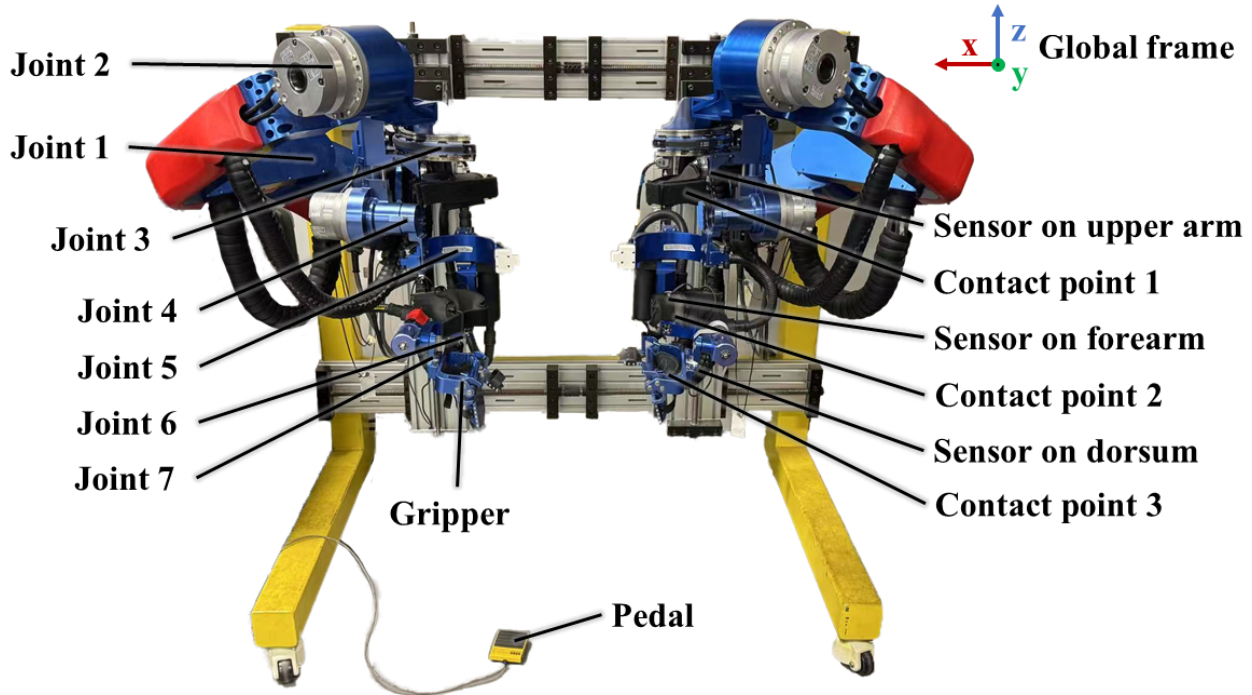


Figure 1.1: EXO-UL8: A dual-arm powered upper-limb exoskeleton.

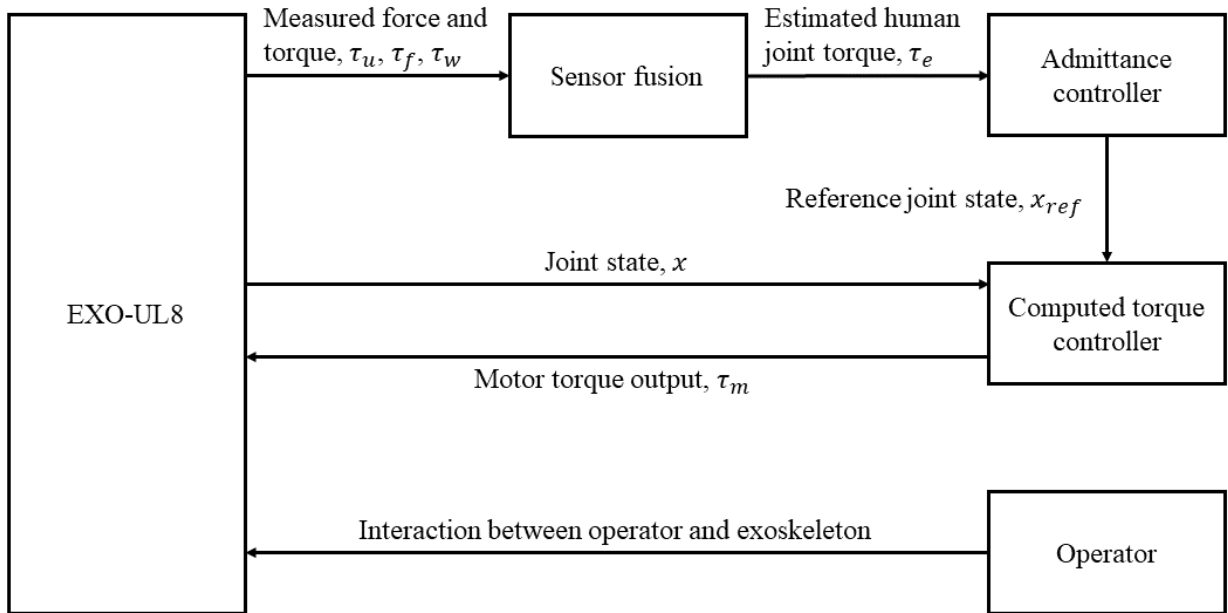


Figure 1.2: Control Scheme of EXO-UL8.

The control scheme of EXO-UL8 is depicted in Figure 1.2. Once the operator wears the

Table 1.1: Anatomical and exoskeleton joint limits.

Joint	DoF	Anatomical Limits	Exoskeleton Limits
1	Shoulder abduction/adduction	180°/30°	90°/0°
2	Shoulder flexion/extension	180°/50°	90°/10°
3	Shoulder internal/external rotation	100°/80°	68.75°/75°
4	Elbow flexion/extension	145°/0°	105°/0°
5	Elbow pronation/supination	85°/90°	70°/39°
6	Wrist flexion/extension	85°/85°	29°/45°
7	Wrist radial/ulnar deviation	15°/45°	29°/30°

exoskeleton, their motion intent is captured by three force/torque sensors. These sensors, located on the upper arm, forearm, and wrist, provide readings denoted as τ_u , τ_f , and τ_w , respectively. These readings are utilized to estimate the human joint torques, τ_e via sensor fusion. Two sensor fusion methods, a hyper parameter-based method and a Kalman filter-based method, are implemented in EXO-UL8. The hyper parameter-based method employs the Jacobian matrix to transform the sensor readings into corresponding joint torques, which are then aggregated through a weighted sum to yield the final joint torque. The Kalman filter-based method applies a Kalman filter to the grouped sensor readings to estimate the joint torque. The estimated joint torque are subsequently used to drive a mass-damping system, generating the reference state for the exoskeleton’s joints, x_{ref} through an admittance controller. To ensure that the exoskeleton’s joint state x accurately follows the reference state, a computed torque controller is implemented to generate motor output τ_m , integrating proportional and differential terms along with gravity and friction compensation.

1.3 Outline

The remaining content is organized as follows:

Chapter 2 reviews current rehabilitation algorithms and identifies their common limitations. Building on this analysis, a self-interactive characteristic is proposed that can selectively provide assistance and resistance to severely and mildly impaired joints, respectively. An experiment is designed to validate this characteristic, and the corresponding results are presented.

Chapter 3 presents a review of the existing literature on redundancy resolution and motion synergy. The proposed study addresses a research gap by investigating motion synergy and redundancy resolution under reduced degrees of freedom in the human arm.

Chapter 4 introduces methods to enhance transparency in human-robot interaction and presents metrics for its quantification. To address the limitations of existing transparency evaluation methods, a new indicator is proposed to reflect the distribution of transparency across different joints. This indicator is then utilized to optimize the weighting and amplifi-

cation of sensor readings. Each chapter concludes with a detailed research plan.

Chapter 5 summarizes the research topics and outlines the overall research timeline.

CHAPTER 2

Upper-Limb Neurological Impairment Rehabilitation Based On Self-Interactive Assist-As-Needed Algorithm

2.1 Introduction

Globally, stroke affects more than 12.2 million individuals each year, making it one of the most pressing medical challenges [1]. In the U.S. alone, around 800,000 new cases occur annually, with stroke remaining a leading cause of disability and mortality [16, 17]. Stroke survivors often suffer from severe motor impairments, such as spasticity, weakness, or paralysis, which drastically impact their ability to perform daily tasks and reduce their overall quality of life [2]. To combat these impairments, active, repetitive, and goal-directed training is essential for motor function recovery [3–5]. Physical therapists are central to this process, guiding patients through exercises designed to rebuild neural pathways [4]. However, with the increasing number of stroke survivors, the intensive time requirements of traditional therapy pose significant challenges [6].

In response to these challenges, rehabilitation robots have become key tools in supporting therapy [7, 8]. These robots offer intensive and sustained therapy, promoting motor recovery through continuous engagement [9]. Research shows that robotic therapy can produce outcomes equal to or better than conventional therapy when delivered at comparable intensities [10, 11]. The advancement of rehabilitation robotics has shifted from simple end-effector robots to high-dimensional exoskeletons that interact with multiple degrees of freedom (DoFs) in the human body, providing sophisticated assistance such as tunnel-like force fields and gravity compensation [18].

A central concept in this field is the "assist-as-needed" (AAN) approach, where robotic devices provide selective assistance, encouraging patients to actively use their affected limbs [14]. However, developing an AAN rehabilitation scheme that can be universally applied to stroke patients with varying degrees of impairment remains a significant challenge. Additionally, the differing levels of impairment across various joints within the affected limbs pose another challenge, as they may require distinct therapeutic approaches. Over the past two decades, numerous approaches to AAN have emerged, including adaptive control to model patient-robot dynamics, force-field control that adapts to the patient's abilities, and disability modeling through Gaussian mixture models (GMM) or radial basis functions (RBF). Despite these efforts, no universally agreed-upon solution for the most effective AAN controller has been established, as each method comes with its own limitations.

This chapter provides a comprehensive overview of the advantages and drawbacks of existing AAN schemes for stroke rehabilitation. Building on this analysis, a novel self-interactive AAN framework is introduced. This framework encompasses trajectory generation, modeling of human arm kinematics and self-interactive characteristic, and a case study, , all aimed at addressing the identified limitations. An experiment is implemented to validate the characteristic, followed by the research plan.

2.2 Literature Review

To achieve optimal therapeutic outcomes in robot-assisted rehabilitation, control algorithms must effectively engage participants [19]. Thus, the minimal assistance should be provided only when necessary, which introduces the concept of assist-as-needed (AAN). A bicycle cranking model, as illustrated in Figure 2.1, is proposed in [20] to explain the assist-as-needed (AAN) mechanism. In this model, the rear wheel represents the patient’s progress in task performance, while the crank symbolizes the therapeutic intervention. The slope of the road reflects the differential between task difficulty and the patient’s motor capability and aids in determining when assistance should be provided. When the road slope is negative, the bicycle coasts on its own, and no additional energy is required for the rear wheel. Conversely, when the slope is positive, the patient may slow down or halt, and thus the crank must supply energy to the rear wheel to maintain progress.

Feedforward and feedback controls and force field are commonly used for AAN. Cai *et al.* [21] compare the implications of band and window AAN control paradigms on gait rehabilitation of regulates shown in Figure 2.2. In the band paradigm, a virtual tunnel is created around a reference trajectory. Within this tunnel, only a velocity tangential to the reference trajectory is present. However, when outside the tunnel, an additional perpendicular velocity component arises. In the window paradigm, tangential force is applied within the moving window. Outside the window, the velocity vector points towards the origin of the window. The authors find that the AAN window paradigm generally demonstrates a higher level of recovery in terms of the number, consistency, and periodicity of steps. Maared *et al.* [20] introduce a Learning from Demonstration (LfD) framework that adjusts task difficulty by evaluating the performance differential between a therapist and a patient. This framework leverages Gaussian Mixture Models (GMM) and Gaussian Mixture Regression (GMR) to represent the desired joint positions or applied forces administered by the therapist. However, this approach does not account for the time-varying capabilities of human subjects. Additionally, a simple PID controller alone cannot guarantee minimal assistance in position-based tasks, as it does not consider the force already applied by the subject. Adaptive controllers are often employed to tailor robot assistance to human motor capabilities. Vergaro *et al.* [23] employ a force field combined with an adaptive controller to enhance participant engagement. They adjusted the force field’s gain based on performance from each trial, ensuring smooth motion—a factor shown to facilitate recovery [24]. Proietti *et al.* [25] integrate model-based gravity compensation with a PD feedback term, allowing

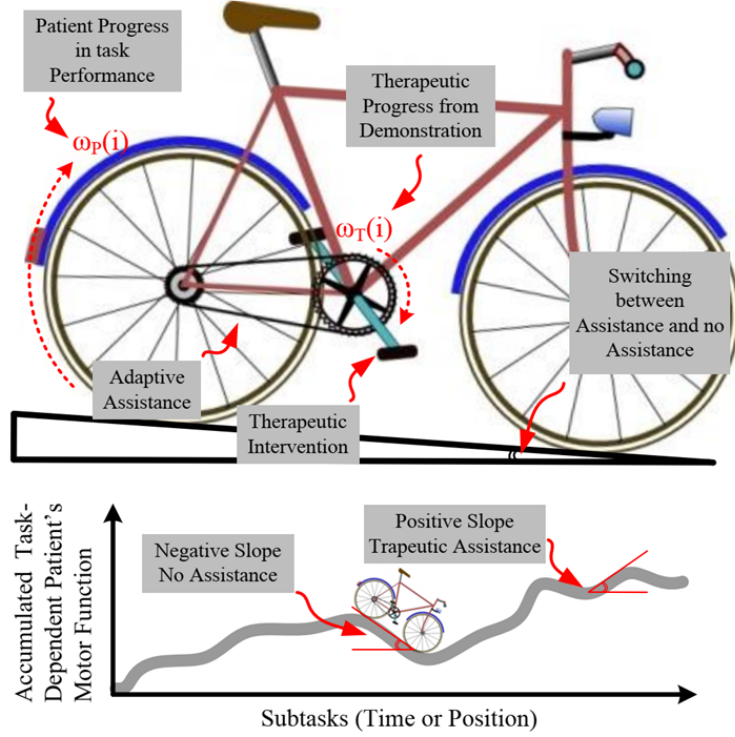


Figure 2.1: Bicycle cranking model [20].

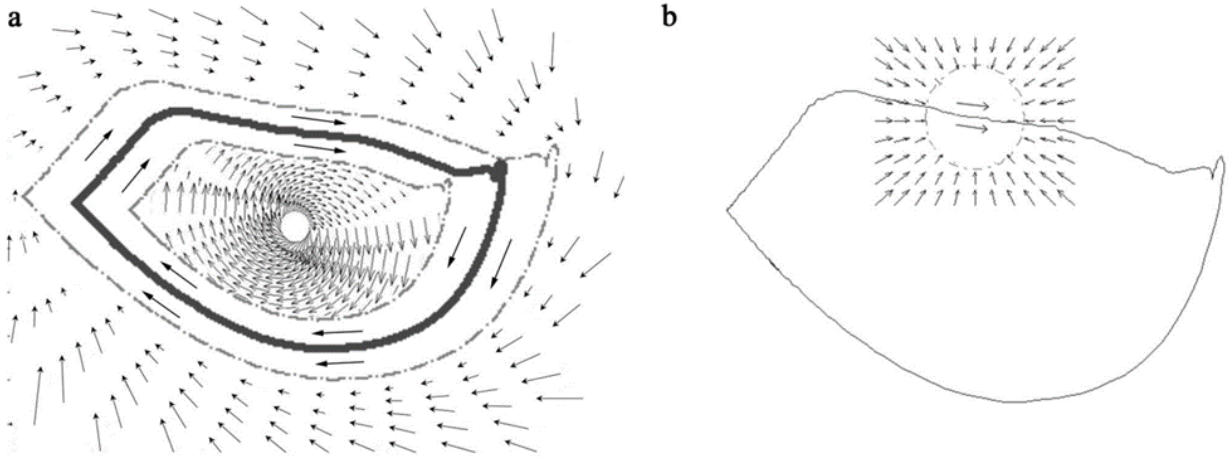


Figure 2.2: Force field generated (a) band paradigm (b) window paradigm [21].

for adaptive adjustments of the gains on a trial-by-trial basis. Wei *et al.* [22] propose a control strategy that combines PID-based feedback with an Iterative Learning Controller (ILC) as shown in Figure 2.3. This approach incorporates an adaptive feedforward term that is updated between trials based on the error between the actual and desired outputs,

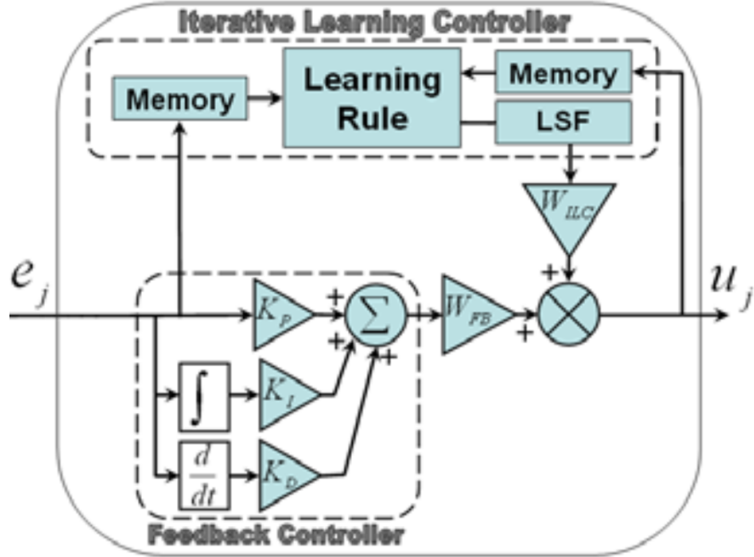


Figure 2.3: Iterative learning controller [22].

transient disturbances introduced in the current trial, and the consistency of the plant and disturbances in the system. Consequently, the controller will not learn when performance is good, will likely avoid learning unwanted disturbances, and will adapt to any consistent disturbance that increases the variance of the error signal. Guo *et al.* [26] developed an adaptive controller that regulates both assistance and resistance based on mean path tracking error and mean velocity from the preceding trial. This controller can switch between assistive and resistive modes dynamically, depending on whether the subject's upper limb position is within or outside a virtual tunnel. These strategies aim to provide either minimal assistance or maximal engagement through trial-by-trial adaptation. However, achieving true minimal assistance remains challenging due to variations in motor capabilities across subjects.

The feasibility of minimal assistance has been debated in [27], suggesting that it is only achievable when the subject's functional capabilities are accurately known. Gaussian Radial Basis Functions (RBFs) are used to represent motor capability and tone within the workspace [28–31]. The approach in [28] features a forgetting term in the adaptive control law, as illustrated in Figure 2.4 to mitigate "slacking" behavior of human motors, though this can perturb subject inputs. Improvements over this method include directionally dependent RBFs applied in [29, 30], which enhance estimation of subjects' motor capabilities compared to [28]. Additionally, the algorithm in [31] adjusts allowable errors while estimating the force exerted by subjects using RBFs. Luo *et al.* [32] utilize a Gaussian RBF network, with its output directly representing participants' modeled capability. A greedy algorithm is used to update the network weights. When the force measured by the sensor exceeds this modeled capability, it suggests that the actual capability may be underestimated. In such cases, the weights are updated to increase the RBF network's output. Conversely, if the measured force is below the modeled capability, it indicates that participants likely have the potential to

exert more force. Thus, the controller maintains the current weights to challenge participants and encourage greater activation effort.

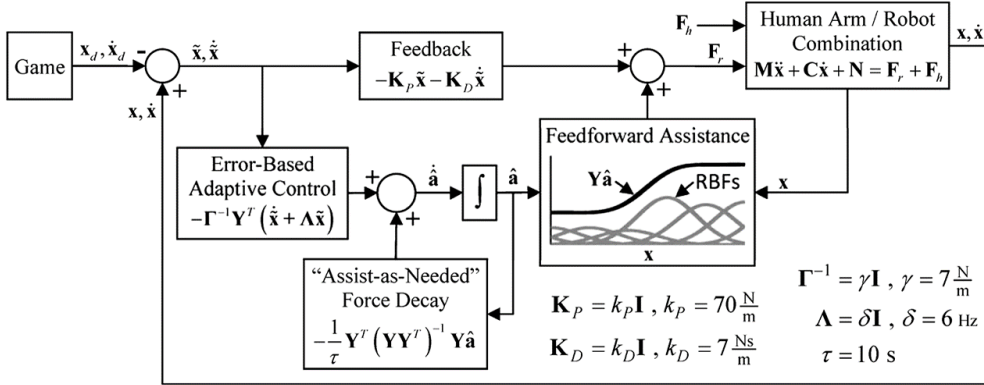


Figure 2.4: Adaptive control based on Gaussian RBFs with a forgetting term (force decay) [28]. The desired state, generated by the designed games, is compared with the current state to produce an error signal. One branch of this error signal is fed into a PD feedback controller, while the other is directed to an adaptive controller. The output of the adaptive controller provides an estimated minimal assistance, which is then assigned to the Gaussian RBFs at the current position. Finally, this estimated assistance is added to the output of the PD controller, and their sum forms the motor command.

For methods utilizing Gaussian RBFs, the assumption is that subjects' capabilities are position-dependent within the workspace. However, this assumption may not hold for neurologically impaired individuals due to the effects of movement disorders [33] and variations in velocity impacting torque production and reach capabilities [34, 35]. Furthermore, the estimation of motor capability based on adaptive control laws requires time to converge, and achieving accurate capability estimation is not assured except under specific conditions [27]. To address these issues, Pehlivan *et al.* [27] model their system as

$$\dot{x} = \hat{F}(x)x + \hat{G}(x)(\tau_r + d - \hat{g}(x)) + n_v \quad (2.1)$$

$$y = Hx + n_w \quad (2.2)$$

where \hat{F} , \hat{G} , and \hat{g} encode the estimated dynamic model, x is the state vector containing the joint position and velocity, y is the measurement vector, H maps the state to the measurement, and n_v and n_w are the process noise and sensor noise, respectively. Then, a Kalman filter (KF) combined with Lyapunov stability analysis is used to estimate the disturbance d , providing fast, stable, and accurate estimation. Despite this, limitations persist regarding constant disturbance assumptions, inertia matrix inversion, and inaccuracies in the plant model that can lead to the inaccuracy of the disturbance estimation [27, 36].

2.3 Research Question

According to [37], assistive therapy is appropriate for patients with severe impairments, while resistive therapy improves movement quality in those with milder impairments. Additionally, the presence of varying impairment levels across different joints within a single patient [38] highlights the need to integrate both therapeutic modes. However, existing algorithms often struggle with effectively transitioning between modes or selectively applying them to the appropriate joints. Moreover, previous methods typically apply assistance to different joints independently, without considering the interaction between them. This interaction can be beneficial, as mildly impaired joints can contribute additional effort to more severely impaired joints, rather than relying entirely on the robot to provide assistance. Hence, the interaction can reduce the robot’s intervention and has the potential to further enhance user engagement. Therefore, a research question could be:

- How can a rehabilitation algorithm be developed to selectively provide both assistance and resistance to the appropriate joints while enhancing the subjects’ engagement by leveraging the interaction across joints?

2.4 Self-Interactive Characteristic

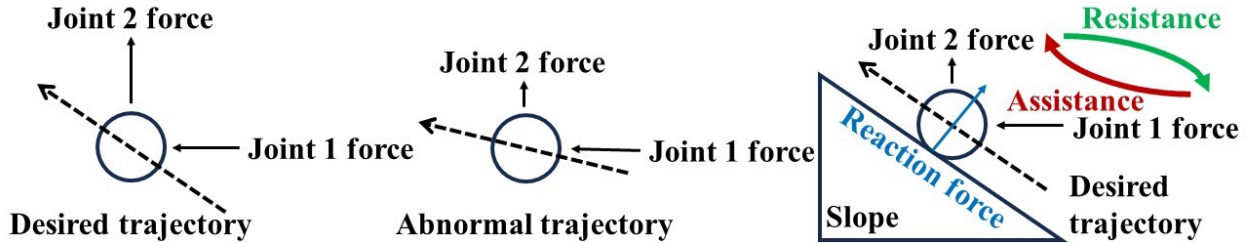


Figure 2.5: Concept of the self-interactive characteristic. Left: both joints have normal capability. Middle: one of the joints has a reduced capability. Right: A slope is added to create a beneficial loop between the two joints.

A novel self-interactive concept is proposed to address the issues outlined above, as abstractly visualized in Figure 2.5. In this visualization, the circle represents a human body part. When both joints function normally, the trajectory follows the dashed line shown in Figure 2.5 (left). If one joint exhibits reduced capability, the trajectory deviates, as illustrated in Figure 2.5 (middle). To counteract these deviations, a slope is introduced using the contact force, as depicted in Figure 2.5 (right). The horizontal component of this force provides natural resistance for the normal joint, while the vertical component assists the joint with reduced capability. This mechanism establishes a beneficial feedback loop: the normal joint aids the impaired joint, and the impaired joint’s need for assistance induces

resistance in the normal joint, all without relying on performance indicators like velocity or positional error. Furthermore, the slope constrains the motion to the desired trajectory, which is crucial as stroke-related motor impairments often require adaptation to a reduced range of movement combinations [39–41], potentially resulting in abnormal behavior.

Based on this concept, two virtual tunnels are utilized—one for the elbow and one for the wrist—to generate contact forces and prevent abnormal motions during the compensation process, assuming rigid arm segments. These virtual tunnels, created by sweeping along desired trajectories with a circular cross-section, function analogously to the slope depicted in Figure 2.5. They allow for free movement of the elbow and wrist within them through a constrained admittance controller. A carefully selected trajectory, informed by the derived model of self-interactive characteristic, maintains the feedback loop shown in Figure 2.5. The desired motion velocity can be adjusted in response to the provided assistance, thereby altering task difficulty. Unlike the other algorithms, the mildly impaired joint will provide some effort to the severely impaired joint according to the capability of the mildly impaired joint. If the joint motor capability proves insufficient despite the contact force, additional assistance will be applied by the exoskeleton, which can further reduce the intervention of the exoskeleton and enhance subjects' engagement.

2.5 Reference Trajectory Generation

Before exploring the specific self-interactive characteristic, it is essential to first generate a reference trajectory along which the virtual tunnel is created. Among the criteria outlined in Section 3.2, most of methods are either validated only in the horizontal or sagittal planes with limited degrees of freedom (DoFs), involve high computational costs, or are exclusively applicable to redundancy resolution. In contrast, the minimum-angular jerk criterion with/without time adjustment [42–44] has been demonstrated to be effective for multi-joint movements in three-dimensional spaces with redundancy. The time adjustment refers to a delay in the elbow motion at the onset of arm movement or an early halt of the elbow motion. In this study, the minimum angular jerk criterion without time adjustment is employed since it has already been demonstrated to yield high accuracy in the absence of joint reversal [44]. However, the primary reason for this choice is that the delay in the elbow motion can hinder the initiation of movement, particularly when the elbow is mildly impaired or healthy.

Only the shoulder abduction/adduction, flexion/extension, internal/external rotation, and elbow flexion/extension are considered for the trajectory generation. The DoFs of the wrist are excluded, as its motion does not theoretically impact the interaction force applied to the wrist. Thus, it does not influence the assistance and resistance experienced by the shoulder and elbow. To generate a trajectory using the minimum-angular-jerk criterion criterion, the cost function C is defined first as follows:

$$C(\theta_i(t)) = \frac{1}{2} \int_{t_s}^{t_f} \ddot{\theta}_i(t)^2 dt = \frac{1}{2} \int_{t_s}^{t_f} \left(\frac{d^3\theta_i(t)}{dt^3} \right)^2 dt \quad (2.3)$$

with boundary conditions:

$$\theta_i(t_s) = \theta_{is} \quad \dot{\theta}_i(t_s) = 0 \quad \ddot{\theta}_i(t_s) = 0 \quad \theta_i(t_f) = \theta_{if} \quad \dot{\theta}_i(t_f) = 0 \quad \ddot{\theta}_i(t_f) = 0 \quad (2.4)$$

where t_s is the start time, t_f is the end time, $\theta_i(t)$ is the angular position of the i^{th} joint t seconds after the start time where $t \in [0, t_f - t_s]$, θ_{is} is the start angular position of the i^{th} joint, and θ_{if} is the final angular position of the i^{th} joint. By applying a technique called the calculus of variations on Equation (2.3) and 2.4, the minimum angular jerk trajectory can be acquired. Let $\mathcal{D}(t)$ be a variation function with the boundary conditions:

$$\mathcal{D}(t_s) = 0 \quad \dot{\mathcal{D}}(t_s) = 0 \quad \ddot{\mathcal{D}}(t_s) = 0 \quad \mathcal{D}(t_f) = 0 \quad \dot{\mathcal{D}}(t_f) = 0 \quad \ddot{\mathcal{D}}(t_f) = 0 \quad (2.5)$$

To minimize $C(\theta_i(t))$, substitute $\theta_i(t)$ in C by $\theta_i(t) + \delta\mathcal{D}(t)$ where δ is a variation operator. Now the cost function becomes

$$C(\theta_i(t) + \delta\mathcal{D}(t)) = \frac{1}{2} \int_{t_s}^{t_f} (\ddot{\theta}_i(t) + \delta\ddot{\mathcal{D}}(t))^2 dt \quad (2.6)$$

Then, the derivative of the new cost function with respect to the variation can be expressed as

$$\frac{dC(\theta_i + \delta\mathcal{D})}{d\delta} = \int_{t_s}^{t_f} (\ddot{\theta}_i + \delta\ddot{\mathcal{D}})\ddot{\mathcal{D}} dt \quad (2.7)$$

When the variation approaches zero,

$$\left. \frac{dC(\theta_i + \delta\mathcal{D})}{d\delta} \right|_{\delta=0} = \int_{t_s}^{t_f} \ddot{\theta}_i \ddot{\mathcal{D}} dt \quad (2.8)$$

By implementing integration by parts,

$$\left. \frac{dC(\theta_i + \delta\mathcal{D})}{d\delta} \right|_{\delta=0} = - \int_{t_s}^{t_f} \mathcal{D} \theta_i^{(6)} dt \equiv 0 \quad (2.9)$$

where $\theta_i^{(6)}$ means the sixth time derivative of θ_i . To make the above property hold true for any variation function \mathcal{D} , $\theta_i^{(6)}$ should equal to zero to minimize the cost function of jerk. Combining the boundary conditions in Equation (2.4) with $\theta_i^{(6)} = 0$, the minimum angular jerk trajectory can be obtained as follows.

$$\theta_i(t) = \theta_{is} + (\theta_{is} - \theta_{if}) \left(15 \left(\frac{t}{t_f - t_s} \right)^4 - 6 \left(\frac{t}{t_f - t_s} \right)^5 - 10 \left(\frac{t}{t_f - t_s} \right)^3 \right) \quad (2.10)$$

$$\theta_i(t) = \theta_{is} + (\theta_{is} - \theta_{if}) (15s^4 - 6s^5 - 10s^3) \quad (2.11)$$

where $s = \left(\frac{t}{t_f - t_s} \right) \in [0, 1]$ is the progress of the motion. The desired angular velocity $\dot{\theta}_i$ can be given as

$$\dot{\theta}_i(t) = \frac{\theta_{is} - \theta_{if}}{t_f - t_s} (60s^3 - 30s^4 - 30s^2) \quad (2.12)$$

With respect to the properties of human arm trajectories, the hand's path and velocity profile remain invariant despite changes in the hand-held load and movement duration [45, 46]. Thus, the advantage of the minimum angular jerk criterion based on Equation (2.11) is that the motion speed can be regulated by assigning new motion durations ($t_f - t_s$) without altering the trajectory shape and velocity profile.

2.6 General Model

2.6.1 Assumptions

The virtual tunnel is established around the referenced trajectory in task space. The advantage of the self-interactive characteristic lies in the ability of multiple joints to influence each other through the interaction forces between the joints and virtual tunnels. This indicates that the method is applicable in scenarios involving more than one engaged joint. However, developing a general model to select feasible trajectories becomes challenging when more than two joints are involved. Since incorporating the self-interactive characteristic establishes the algorithm as a new branch within the AAN field, this study starts by analyzing cases involving flexing motion of two engaged joints (shoulder flexion/extension and elbow flexion/extension) in a parasagittal plane.

2.6.2 Cross-Section Shape of the Virtual Tunnels

In the case of a circular cross-section, the wrist and elbow positions are dependent on the contact forces. In contrast, a rectangular cross-section can decouple the contact forces from the wrist and elbow positions when they contact the corners of the tunnel. Consequently, in a circular cross-section, the wrist and elbow can move along the bound of the cross-section as the contact force components vary. In a rectangular cross-section, the wrist and elbow tend to remain in the corner unless the contact forces direct them toward another corner. Overall, the circular cross-section allows for greater variation in movement, which may facilitate motor function recovery [47]. Therefore, the circular cross-section is adopted in this study.

2.6.3 Arm Kinematics

The frames of each joint are attached in Figure 2.6 (left). Frame 0 is the base frame, frame 1 corresponds to shoulder abduction/adduction, frame 2 to shoulder flexion/extension, frame 3 to shoulder internal/external rotation, frame 3' to an intermediate frame used to assign frame 4, frame 4 to elbow flexion/extension, frame 5 to the wrist, frame u to the center of mass of the upper arm, and frame f to the center of mass of the forearm. The angular positions of the joints associated with frames 1, 2, 3, and 4 which correspond to the four degrees of freedom of the shoulder and elbow, are denoted as θ_1 , θ_2 , θ_3 , and θ_4 . The rest

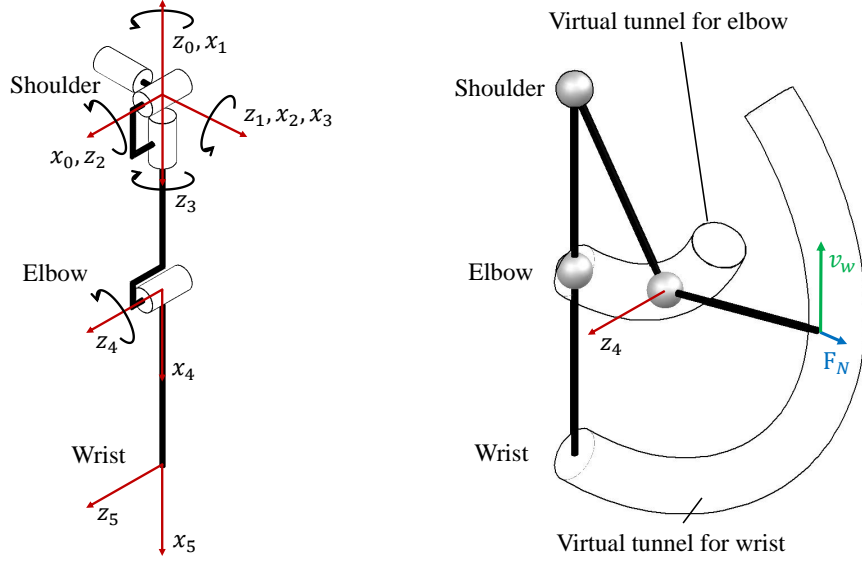


Figure 2.6: The arm model (left) and virtual tunnels (right).

of the frames are static and correspond to intermediate frames or the frames attached at points of interest. The lengths of the upper arm and forearm are represented by l_u and l_f , respectively.

The Denavit-Hartenberg parameters (DH parameters) are displayed in Table 2.1. Ac-

Table 2.1: DH parameters of the arm model

Frame $i - 1$	Frame i	α_{i-1}	a_{i-1}	d_i	θ_i
0	1	-90°	0	0	-90° + θ_1
1	2	-90°	0	0	-90° + θ_2
2	3	90°	0	0	θ_3
3	3'	-90°	0	0	-90°
3'	u	0°	l_{cmu}	0	0°
3'	4	0°	l_u	0	θ_4
4	f	0°	l_{cmf}	0	0°
4	5	0°	l_f	0	0°

cording to the DH parameters, the transformation matrix from frame $i - 1$ to frame i , T_i^{i-1} can be expressed as

$$T_i^{i-1} = \begin{bmatrix} \cos(\theta_i) & -\sin(\theta_i) & 0 & a_{i-1} \\ \sin(\theta_i) \cos(\alpha_{i-1}) & \cos(\theta_i) \cos(\alpha_{i-1}) & -\sin(\alpha_{i-1}) & -d_i \sin(\alpha_{i-1}) \\ \sin(\theta_i) \sin(\alpha_{i-1}) & \cos(\theta_i) \sin(\alpha_{i-1}) & \cos(\alpha_{i-1}) & d_i \cos(\alpha_{i-1}); \\ 0 & 0 & 0 & 1 \end{bmatrix} \quad (2.13)$$

The transformation matrix from frame i to frame n , T_n^i can be obtained by chain rule, as shown below.

$$T_n^i = T_j^i T_k^j T_m^k \cdots T_n^h = \begin{bmatrix} R_n^i & p_n^i \\ \mathbf{0} & 1 \end{bmatrix} \quad (2.14)$$

where R_n^i and p_n^i are the rotation matrix and position vector pointing from frame i to frame n , respectively.

2.6.4 Properties of Self-Interactive Characteristic

Self-interactive characteristic refers to the condition in which the torque induced by contact forces acts assistively on severely impaired joints—those with significantly limited range of motion or motor capability—and resistively on mildly impaired joints that retain most motor functions. A closed virtual tunnel is constructed around the desired trajectory of the elbow, with another tunnel similarly built around the wrist’s trajectory in task space. Abnormal coupling between shoulder and elbow movements, often referred to as pathological muscle synergies, is frequently observed following neurological injury [40, 48, 49]. Constructing tunnels for both the shoulder and elbow helps constrain the arm to a more natural configuration.

For the scenario where the wrist and/or elbow are moving along the surface of their corresponding virtual tunnels, suppose that the joint angular velocity is $\dot{q}_h = [\dot{\theta}_1 \ \dot{\theta}_2 \ \dot{\theta}_3 \ \dot{\theta}_4]^T$ at a certain configuration $q_h = [\theta_1 \ \theta_2 \ \theta_3 \ \theta_4]^T$.

For the contact force on the elbow, if shoulder adduction/abduction and flexion/extension are not engaged simultaneously, it will cause no assistance or resistance to any joints, regardless of whether the shoulder internal/external rotation and elbow flexion/extension are engaged. Joint i is considered to receive assistance if the torque acting on it performs positive work. Conversely, the joint experiences resistance if the torque performs negative work.

Property 1. If $\|\dot{\theta}_1 \ \dot{\theta}_2\|^T \|0 < 2$, then $\tau_{ei}\dot{\theta}_i = 0$, $\forall i \in 1, 2, 3, 4$.

Notation: τ_{ei} denotes the torque at the i^{th} joint induced by the contact force on the elbow.

Proof. For the contact between the elbow and its corresponding virtual tunnel in the scenario mentioned above, the linear velocity of the elbow v_e , which is tangential to the surface of the virtual tunnel, is given by:

$$v_e = J_{ve}(q_h)\dot{q}_h \quad (2.15)$$

where $J_{ve}(q_h) \in \mathbb{R}^{3 \times 4}$ is the partial Jacobian of the elbow at the configuration q_h with a column of zeros at the end. Let the contact force acting on the elbow be $F_e = [f_{e1} \ f_{e2} \ f_{e3}]^T$, which is perpendicular to the corresponding tunnel’s surface. The torque induced by the

contact force on the elbow, τ_e can be obtained as follows.

$$\tau_e = J_{ve}^T F_e = \begin{bmatrix} -l_u c_2 (f_{e1}c_1 - f_{e3}s_1) \\ l_u (f_{e2}c_2 + f_{e3}c_1s_2 + f_{e1}s_1s_2) \\ 0 \\ 0 \end{bmatrix} \quad (2.16)$$

where s_i and c_i represent $\sin \theta_i$ and $\cos \theta_i$, respectively, where $i = 1, 2, 3, 4$. The first two elements in τ_e can be non-zero when shoulder adduction/abduction and flexion/extension are engaged simultaneously. For example, the elbow moves along a slope as shown in Fig. 2.5, where the upper arm is not parallel to the surface of the slope. Besides, the contact force on the elbow is also perpendicular to the linear velocity of the elbow v_e . Hence, the power of the contact force on the elbow P_e should be zero, as shown in the following equation.

$$P_e = F_e^T v_e = F_e^T J_{ve} \dot{q}_h = \tau_e^T \dot{q}_h = \sum_i \tau_{ei} \dot{\theta}_i = 0 \quad (2.17)$$

where τ_{ei} is the i^{th} element of τ_e . From equation (2.16), the power of the elbow contact-induced torque for the shoulder internal/external rotation and the elbow is always zero. When neither the shoulder adduction/abduction nor flexion/extension is engaged, equation (2.17) can be maintained. When one of the shoulder adduction/abduction or flexion/extension is engaged, the angular velocity of the other will be zero. To preserve equation (2.17), the power generated by the elbow contact-induced torque on the engaged shoulder adduction/abduction or flexion/extension must also be zero. Based on the analysis of these cases, we can conclude that the contact force on the elbow does not cause assistance or resistance to any joints, irrespective of the states of shoulder internal/external rotation and elbow flexion/extension, if shoulder adduction/abduction and flexion/extension are not engaged at the same time. \square

If any joints receive assistance from the elbow and wrist contact, then at least one other joint must necessarily experience resistance, as shown in Property 2.

Property 2. if $S_a \neq \emptyset$, then $\tau_i \dot{\theta}_i > 0$, $i \in S_a \wedge \tau_j \dot{\theta}_j < 0$, $\exists j \notin S_a$.

Notation: S_a denotes the set of indices corresponding to joints that receive assistance, and τ_i denotes the total torque at the i^{th} joint induced by the elbow and wrist contact.

Proof. For the contact between the wrist and its corresponding virtual tunnel, the linear velocity of the wrist v_w , which is tangential to the surface of the virtual tunnel, is given by:

$$v_w = J_{vw}(q_h) \dot{q}_h \quad (2.18)$$

where $J_{vw}(q_h) \in \mathbb{R}^{3 \times 4}$ is the partial Jacobian of the wrist at the configuration q_h . The torque induced by the contact force on the wrist, τ_w , can be expressed as follows.

$$\tau_w = J_{vw}^T F_w \quad (2.19)$$

where J_{ve} and $J_{vw} \in \mathbb{R}^{3 \times 4}$ are the partial Jacobian of the elbow and the wrist.

The contact force on the wrist F_w should be perpendicular to the surface of the virtual tunnel due to the geometry of the tunnel. Thus, it is also perpendicular to the linear velocity of the wrist $v_w \in \mathbb{R}^3$ in this scenario. Therefore, the power of the contact force on the wrist P_w can be expressed as:

$$P_w = F_w^T v_w = F_w^T J_{vw} \dot{q}_h = \tau_w^T \dot{q}_h = \sum_i \tau_{wi} \dot{\theta}_i = 0 \quad (2.20)$$

where τ_{wi} denotes the torque at the i^{th} joint induced by the contact force on the wrist. From equation (2.20), the torque induced by the wrist contact does not perform net work on the arm. The total torque induced by the contact on the elbow and wrist, τ can be given by $\tau_e + \tau_w$. The total power of the contact on the elbow and wrist P_{tot} can be given as:

$$P_{tot} = P_e + P_w = \sum_i (\tau_{ei} + \tau_{wi}) \dot{\theta}_i = \sum_i \tau_i \dot{\theta}_i = 0 \quad (2.21)$$

To satisfy equation (2.21), if the torque on any engaged joint performs positive power, the torque on at least one other engaged joint must perform negative power to offset it, as expressed by $\sum_{i \in S_a} \tau_i \dot{\theta}_i + \sum_{i \in S_r} \tau_i \dot{\theta}_i = 0$ where S_r denotes the set of indices corresponding to joints that experience resistance. \square

From **Property 2**, it becomes essential to design strategies ensuring that positive work is directed to severely impaired joints while negative work is absorbed by mildly impaired ones. Gravity can influence the generation of trajectories intended to exploit self-interactive characteristic. Inappropriately designed trajectories may allow gravity to assist certain joints, thereby diminishing the effectiveness of self-interaction and potentially leading to subject disengagement or relaxation. Therefore, the set of trajectories of two joints that effectively leverage self-interactive characteristic, denoted as \mathfrak{T} , can be defined as

$$\mathfrak{T} = \{ \mathbf{x}_{i,j}(t) \mid t \in [t_s, t_f], i \neq j, \mathcal{C}(i, j, t) \} \quad (2.22)$$

where i and j are the indices of the two joints of interest, $\mathbf{x}_{i,j}$ is the trajectory of the two joints, the condition $\mathcal{C}(i, j, t)$ is given by:

$$\mathcal{C}(i, j, t) := \left[\begin{array}{l} \left(\tau_i(t) \dot{\theta}_i(t) \geq 0 \wedge \tau_i(t) \dot{\theta}_i(t) \leq 0 \right) \\ \wedge \left(\tau_j(t) \dot{\theta}_j(t) \geq 0 \wedge \tau_j(t) \dot{\theta}_j(t) \leq 0 \right) \end{array} \right] \quad (2.23)$$

The condition $\mathcal{B}(i)$ becomes effective when there exists a difference in impairment levels, and it may vary with the arm state, as joint impairments can be state-dependent. This condition is stringent, as the trajectory is designed for general applicability without prior knowledge of individual impairment distributions across joints. However, if such impairment

levels are known in advance, the condition can be appropriately relaxed. In addition, singularities may cause the arm to become trapped at certain positions within the virtual tunnel during practical implementation. Therefore, trajectory generation must be conducted with caution to ensure safe and consistent performance.

2.6.5 Case Study

Since the self-interactive characteristic represent a novel concept, a simple case is studied in which the interaction between shoulder flexion/extension and elbow flexion/extension is considered, while other degrees of freedom (DoFs) are fixed. The arm motion is constrained to a parasagittal plane. The initial configuration of the arm $q_{hs} = [\theta_1 \ \theta_2 \ \theta_3 \ \theta_4]^T$ in this paper is defined as $[0^\circ \ 0^\circ \ 0^\circ \ 40^\circ]^T$, while the final configuration q_{hf} is defined as $[0^\circ \ 60^\circ \ 0^\circ \ 100^\circ]^T$. The desired trajectory is then generated using equations (2.11) and (2.12). In this case, the virtual tunnels are constructed on a two-dimensional plane, with their cross sections represented as rectangles of zero width. The radius (or the half length) of the cross section of the virtual tunnels r_{vt} is set to be sufficiently small to assume that the arm's actual motion closely follows the desired path defined by the initial and final configurations above. Besides, in this case, according to Property 1, the tunnel for the elbow provides neither assistance nor resistance; therefore, only the contact at the wrist is considered.

The contact force acting on the wrist $F_w \in \mathbb{R}^3$ can be decomposed into two orthogonal components lying in a plane that is perpendicular to v_w . Since $\dot{\theta}_1$ and $\dot{\theta}_3$ are zero for the motion, the wrist contact induced torque τ_w can be expressed as:

$$\begin{aligned}\tau_w &= J_{vw}^T f_{w1} \frac{v_w \times \hat{n}_r}{\|v_w \times \hat{n}_r\|} + J_{vw}^T f_{w2} \hat{n}_r \\ &= \begin{bmatrix} -f_{w2} (l_f c_{24} + l_u c_2) \\ f_{w1} l_f l_u s_4 \dot{\theta}_4 \Psi^{-1}(q_h, \dot{q}_h) \\ f_{w2} l_f s_4 \\ -f_{w1} l_f l_u s_4 \dot{\theta}_2 \Psi^{-1}(q_h, \dot{q}_h) \end{bmatrix}\end{aligned}\quad (2.24)$$

where f_{w1} and $f_{w2} \in \mathbb{R}$ denote the combination of the magnitude and polarity of the two components of F_w , respectively. The absolute values of f_{w1} and f_{w2} represent the magnitude and their sign represents the polarity. The sign is positive if the real force component is in the default direction of the components $\frac{v_w \times \hat{n}_r}{\|v_w \times \hat{n}_r\|}$ and \hat{n}_r , and negative otherwise. \hat{n}_r can be any unit vector that is not parallel with v_w , and it is set as $[1 \ 0 \ 0]^T$ in this paper.

The term c_{ij} denotes $\cos(\theta_i + \theta_j)$, and $\Psi(q_h, \dot{q}_h)$ is a term that is always positive for the motion studied. Since only the flexion/extension motion of the shoulder and elbow is engaged, the second and fourth elements in τ_w are focused.

There are four possible cases of the impairment conditions to validate that the desired trajectory is inside \mathfrak{T} :

2.6.5.1 Severely Impaired Shoulder and Mildly Impaired Elbow

In this case, the wrist heuristically contacts the upper half of the cross-section of its corresponding tunnel. As a result, $\text{sign}(f_{w1})$ is positive. Additionally, in equation (2.24), $\dot{\theta}_2$, $\dot{\theta}_4$, s_2 , c_2 , and s_4 are all non-negative. Therefore, the contact-induced force at the shoulder flexion/extension joint performs positive work, while the force at the elbow flexion/extension joint performs negative work.

2.6.5.2 Mildly Impaired Shoulder and Severely Impaired Elbow

In this case, the wrist heuristically contacts the lower half of the cross-section of its corresponding tunnel. As a result, $\text{sign}(f_{w1})$ is negative. Furthermore, $\dot{\theta}_2$, $\dot{\theta}_4$, s_2 , c_2 , and s_4 remain non-negative in equation (2.24). Consequently, the contact-induced force at the shoulder flexion/extension joint performs negative work, while the force at the elbow flexion/extension joint performs positive work.

2.6.5.3 Severely Impaired Shoulder and Elbow

In this situation, the self-interactive characteristic has minimal effect. Our algorithm can operate similarly to a standard minimal assist-as-needed algorithm, providing assistance to both joints.

2.6.5.4 Mildly Impaired Shoulder and Elbow

In this case, the self-interactive characteristic has minimal impact, and the task difficulty can be increased by raising the desired motion speed, thereby positioning the subjects' performance within the first three categories. Additionally, the control mode can be switched to one that provides resistance to both joints.

2.7 Virtual Tunnel Creation

Since the low-level controller tracks the reference state output from the high-level controller, the reference state should be constrained to make the elbow and wrist inside their corresponding tunnels. The reference joint velocity \dot{q}^{ref} is modified and the modified reference joint velocity \dot{q}_m^{ref} can be obtained as follows [50].

$$\begin{aligned} \min \quad & \|\dot{q}_m^{ref} - \dot{q}^{ref}\|_2^2 \\ \text{s.t.} \quad & \hat{n}_e J_{ve} \dot{q}_m^{ref} \geq 0, \\ & \hat{n}_w J_{vw} \dot{q}_m^{ref} \geq 0 \end{aligned} \tag{2.25}$$

where \hat{n}_e which can be \hat{n}_{ne} or \hat{n}_{te} is the direction of the contact force on the elbow from the tunnels' side wall or the cap, and \hat{n}_w which can be \hat{n}_{nw} or \hat{n}_{tw} is the direction of the contact

force on the wrist from the tunnels' side wall or the cap. The updated position q_m^{ref} is given as:

$$q_m^{ref} = q^{ref} - (q^{ref} - q_{m,old}^{ref}) \cdot \hat{n}_v \hat{n}_v \quad (2.26)$$

where $q_{m,old}^{ref}$ is the reference joint position in previous time step, and \hat{n}_v is acquired by:

$$\hat{n}_v = \frac{\dot{q}^{ref} - \dot{q}_m^{ref}}{\|\dot{q}^{ref} - \dot{q}_m^{ref}\|} \quad (2.27)$$

This method constrains velocity to serve as the basis for position correction, eliminating the need for inverse kinematics.

2.8 Validation of Self-Interactive Characteristic

To more accurately simulate the natural interaction between the human arm and the virtual tunnel, this experiment employed the constrained admittance control, excluding virtual assistance. The initial configuration was defined as shoulder flexion at 0° and elbow flexion at 40° , while the final configuration corresponded to shoulder flexion at 60° and elbow flexion at 100° as shown in Figure 2.7. The remaining degrees of freedom (DoFs) of the arm were maintained at zero.

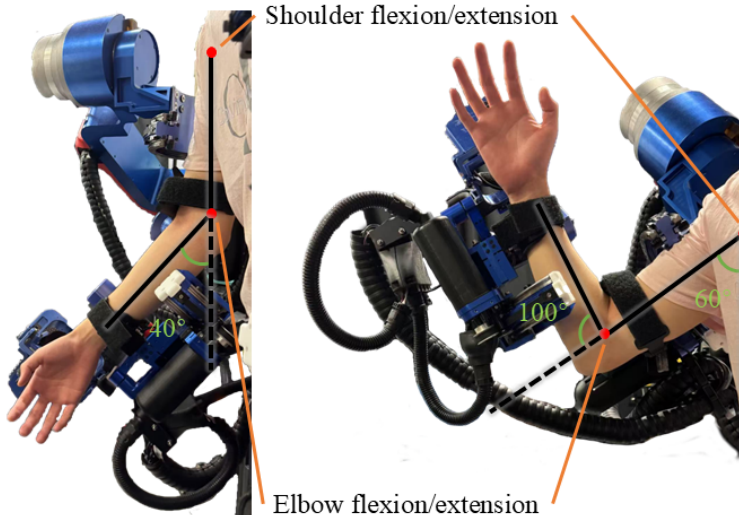


Figure 2.7: Task for shoulder and elbow flexion/extension.

The subjects performed several practice runs to familiarize themselves with the exoskeleton. Three conditions were designed for this section: 1) BA (Both Active): Both joints are active; 2) ASPE (Active Shoulder, Passive Elbow): The shoulder is active, and the elbow is passive; 3) PSAE (Passive Shoulder, Active Elbow): The shoulder is passive, and the elbow is active. An elastic brace was placed on the passive joint to assist subjects in maintaining

relaxation of that joint. The subjects were instructed to track the desired angular position of the active joint from the initial configuration to the final configuration within approximately 3 seconds for five trials in each condition, as regulated by a metronome. After a brief rest, the task was repeated with the goal of completing it within approximately 6 seconds for another five trials. The readings from the two F/T sensors were recorded.

The general theory of contact between the human arm and virtual tunnels is discussed above. However, when wearing the exoskeleton, the interaction force between the human arm and the exoskeleton differs from the contact force between the human arm and the virtual tunnels due to imperfect transparency. Specifically, the interaction force primarily reflects the user's motion intention in both free-motion and constrained directions. The force driving human motion intention contributes to imperfect transparency, while in constrained directions, the interaction force is effectively neutralized by the virtual tunnels.

To validate the self-interactive characteristic, the torque arising from the contact force between the human arm and the virtual tunnels must be separated from the torque resulting from the interaction between the human arm and the exoskeleton. The constrained state can be used to derive the motion intention in the free-motion direction, denoted as τ_f , through an inverse admittance controller and inverse sensor fusion process. Thus, the torque due to the contact force between the human arm and the virtual tunnels, τ_c , can be calculated as follows:

$$\tau_c = \tau_{tot} - \tau_f \quad (2.28)$$

where τ_{tot} represents the total torque induced by the human-exoskeleton interaction. However, this is typically not feasible since the sensor fusion process is generally non-invertible. Fortunately, in both the slow and fast trials, the total torque in the healthy condition can effectively represent the human motion intention in the free-motion direction, as no virtual tunnels are present. This torque in the healthy condition can also represent the motion intention in the free-motion direction for the impaired cases, as the subjects are instructed to perform the same task within nearly identical time frames. Therefore, the contact-induced torque, τ_c , can be quantified as the difference between the total torque in the impaired cases and that in the healthy condition.

The total torque τ_{tot} for the slow and fast trials is illustrated in Figure 2.8. Since both $\dot{\theta}_2$ and $\dot{\theta}_4$ are positive in the experiment, the sign of the torque directly indicates whether the interaction force between the human subject and exoskeleton performs assistive or resistive work. For the shoulder, the difference between MSSE torque and healthy torque is predominantly negative, indicating that the contact force between the human subject and virtual tunnel induces resistance on the mildly impaired shoulder. Conversely, the difference between SSME torque and healthy torque is mostly positive, suggesting that the contact force provides assistance to the severely impaired shoulder.

For the elbow, the difference between MSSE torque and healthy torque is primarily positive, implying that the contact force assists the severely impaired elbow. In contrast, the difference between SSME torque and healthy torque is generally negative, indicating that the contact force induces resistance on the mildly impaired elbow.

Notably, even the raw interaction force between the human subject and the exoskeleton—including resistance caused by imperfect transparency—can still generate assistive and resistive torques on the appropriate joints. Due to the synergistic motion of the human arm, completely isolating the effort of one joint from another may be infeasible, and it is particularly challenging for any joint to remain entirely relaxed. This experiment phenomenon is acceptable, as a severely impaired joint may still be capable of exerting some effort in actual patients. Hence, as shown in Figure 2.8, the magnitude of the assistive torque does not exhibit significant variation with increasing motion speed, whereas the magnitude of the resistive torque increases with speed. However, the key observation is that motion speed does not influence the torque direction in this study, even in the presence of imperfect transparency in the admittance controller or the limited capability of a severely impaired joint. This finding aligns with Equation (2.24). The primary reason is that, under the trajectory employed in this study, variations in motion speed do not alter the default contact force direction, and the joint motion direction remains unchanged.

2.9 Validation of Virtual Tunnel Creation

The virtual tunnel is defined at the kinematic level in the experiment used to validate the self-interactive characteristic, with the constrained reference trajectory and the actual wrist trajectory, both transformed into Cartesian space, shown in Fig. 2.9. The virtual tunnel is defined at the kinematic level, and the constrained reference trajectory and the actual trajectory of the wrist of subject 2 transformed into Cartesian space using the data from the experiment, are depicted in Fig. 2.9. The results of the other subjects are similar to the one shown here. Only the wrist trajectory is plotted since the arm motion is constrained within a parasagittal plane in this study, ensuring that the elbow never contacts its corresponding tunnel. When the arm contacts the virtual tunnel, no significant oscillatory dynamic response of the reference state is induced, because the velocity component in the unexpected direction is directly eliminated, functioning similarly to a perfectly inelastic collision. The reference trajectory remains well-constrained within the tunnel boundaries, and the actual trajectories closely follow the reference. The arm makes contact with the virtual tunnel at 34.12%, 36.46%, and 39.46% time progress in the ASPE, PSAE, and BP conditions, respectively. This aligns with the velocity discontinuities observed in Fig. 2.9d. Since the velocity follows a bell-shaped profile with small magnitudes at both the beginning and end of the movement, the arm, despite contacting the tunnel at a non-negligible time progress, remains in contact for approximately 79.19%, 70.52%, and 71.29% of the total motion range for ASPE, PSAE, and BP conditions. This prolonged contact enables the system to exploit self-interactive characteristic over a substantial portion of the movement. This portion can be tuned by modifying the radius of the virtual tunnel. This adjustment may also serve as a future direction for enhancing the efficiency of self-interactive characteristic and identifying optimal trajectories.

This method of creating virtual tunnels improves motion smoothness compared to dynamic-

level approaches, which can be beneficial for motor recovery [24]. Besides, constraining the arm motion within a predefined region enhances safety by preventing excessive movements and reducing the risk of injuries. The virtual tunnels, with a certain width, are used in conjunction with the compliant control scheme in this paper, allowing for motion variations while maintaining guidance, which further supports motor recovery [47].

Only the wrist trajectory is plotted, as the arm motion is constrained to a parasagittal plane in this study, ensuring that the elbow does not come into contact with its corresponding tunnel. When the arm interacts with the virtual tunnel, no significant oscillatory dynamic response occurs, as the velocity component in the unexpected direction is immediately eliminated, resembling a perfectly inelastic collision. The reference trajectory remains well-constrained within the tunnel boundaries, and the actual trajectories closely follow the reference regardless of the motion speed. This approach to creating virtual tunnels enhances motion smoothness compared to dynamic-level methods, which is beneficial for motor recovery [24]. Additionally, restricting the arm's movement within a predefined region enhances safety by preventing excessive motion and reducing the risk of injury. The virtual tunnels, which have a certain width, are employed along with my compliant control scheme in this paper, allowing for motion variations while still providing guidance, further supporting motor recovery [47].

2.10 Research Plan

An algorithm will be developed to adjust the task difficulty based on the subject performance and mitigate the effect of the insufficient voluntary capability based on the error change over time. After that, an experiment will be set up to validate the task difficulty adjustment algorithm. Finally, the proposed algorithm will be compared with a baseline controller without using the self-interactive characteristic to demonstrate that the assistance provided by the exoskeleton is reduced using our algorithm.

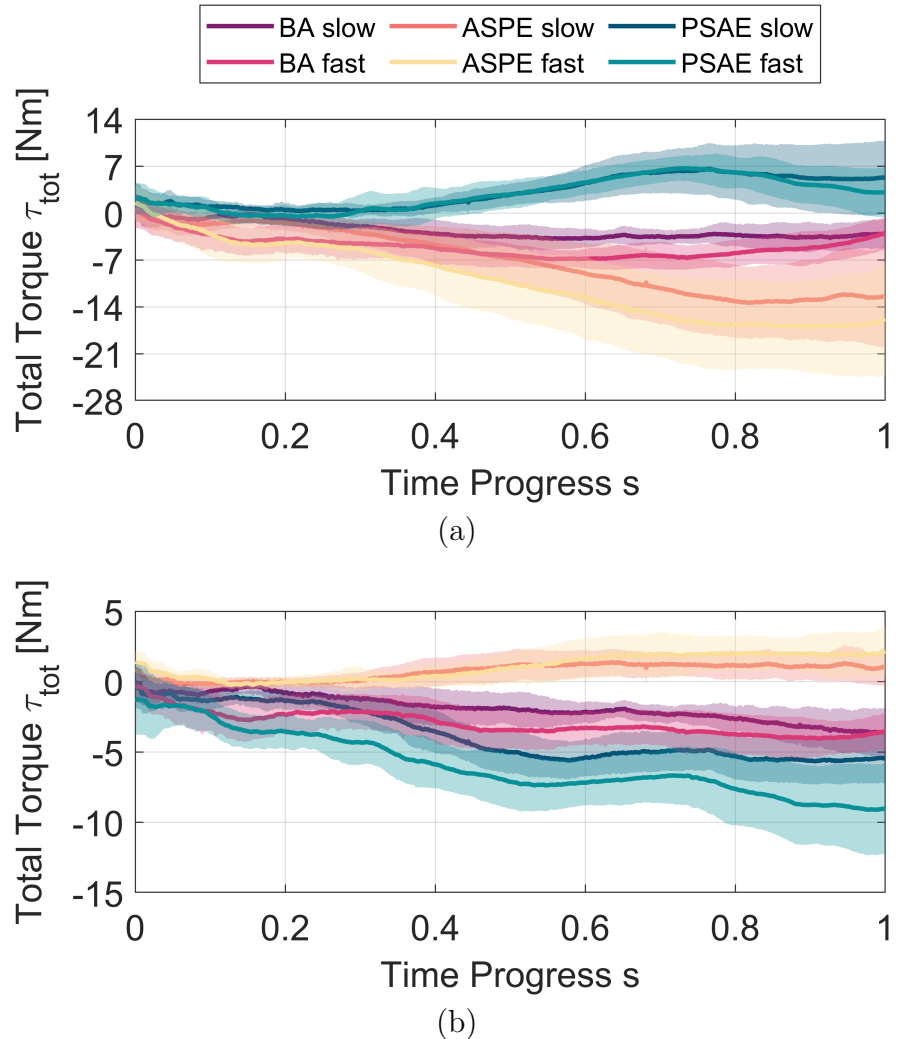


Figure 2.8: Total interactive torque over time for slow trials. (a) Torque on the shoulder.
(b) Torque on the elbow.

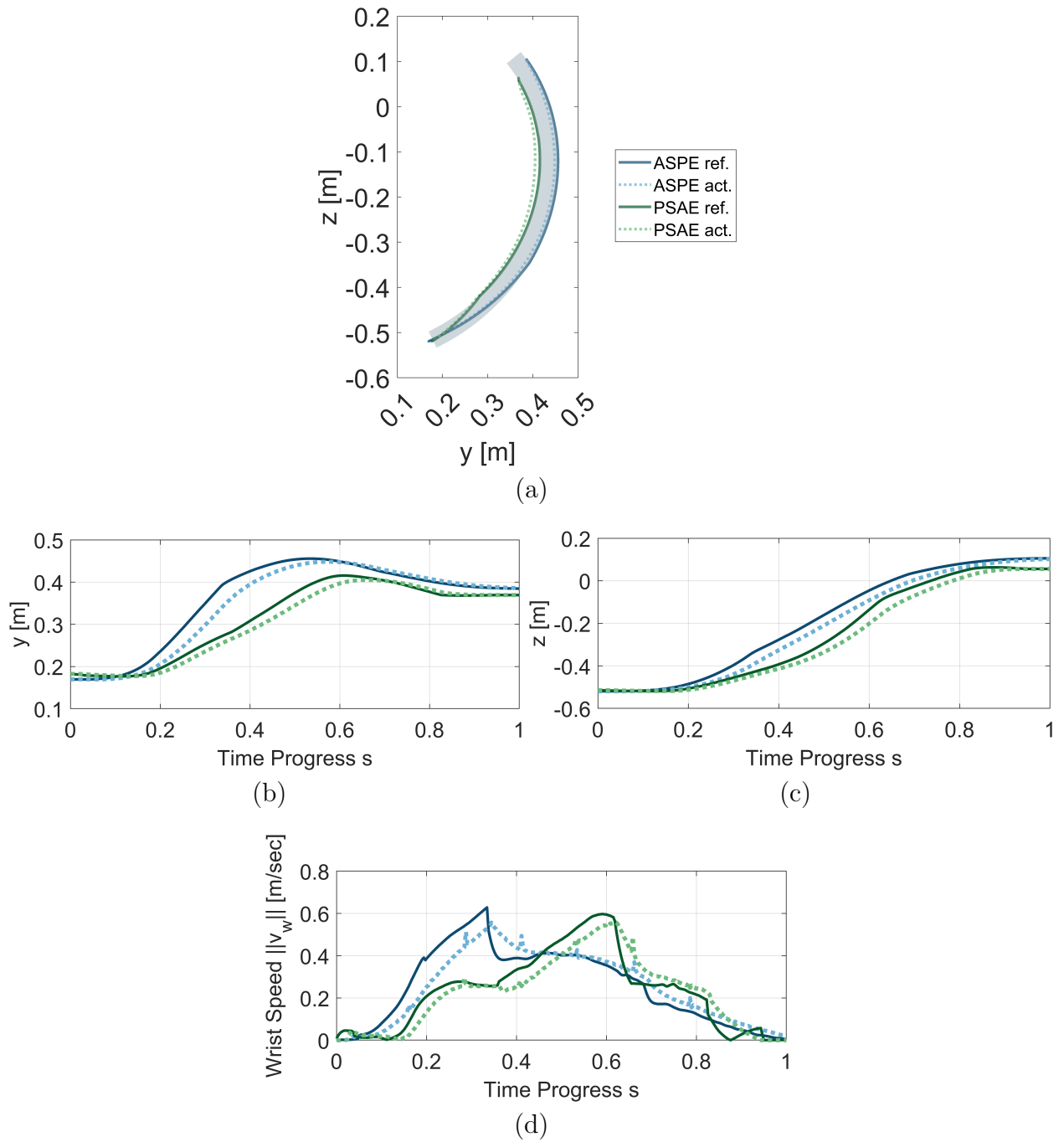


Figure 2.9: Reference and actual state of the wrist of subject 2 in one of the fast trials. (a) Trajectory of the wrist (b) Wrist position in y-axis with respect to time (c) Wrist position in z-axis with respect to time (d) Wrist speed with respect to time.

CHAPTER 3

Upper-limb Redundancy Resolution

3.1 Introduction

The human arm exhibits remarkable dexterity due to its seven degrees of freedom (DoFs), which allow for redundancy in movement execution. While only six DoFs are required to position and orient the wrist in space, the additional DoF enables multiple configurations to achieve the same task. This redundancy poses both a challenge and an opportunity in motor control, particularly in the context of human-robot interaction and rehabilitation. Understanding how the human nervous system resolves redundancy is crucial for designing assistive technologies, such as wearable exoskeletons, that can seamlessly integrate with natural movement patterns.

Numerous studies have explored criteria for redundancy resolution, including minimum-jerk, minimum-torque change, and minimum-work principles. However, these approaches often focus on simplified two-dimensional scenarios and may not fully account for redundancy in complex, three-dimensional tasks. Recent research has investigated more sophisticated models incorporating joint dependencies, time-adjusted motion planning, and multi-criteria optimization, yielding insights into human-like trajectory generation.

Beyond redundancy resolution, synergy-based control has emerged as a key concept in understanding human motor coordination. Studies suggest that the nervous system does not control each DoF independently but rather utilizes synergies—coordinated patterns of muscle activation or joint movement—to simplify control. Evidence from electromyographic (EMG) analysis and kinematic studies has demonstrated that a small number of principal components can explain a significant proportion of movement variability, supporting the idea that synergies underlie human motion.

By investigating arm movement under progressively constrained redundancy, this study aims to uncover how synergies emerge and adapt in response to joint limitations. Such findings will not only advance the theoretical understanding of motor control by revealing how the nervous system reorganizes movement strategies under joint constraints, but also provide crucial insights for designing exoskeletons and rehabilitation protocols. In exoskeleton design, understanding synergies can help create control strategies that assist users in a way that aligns with their natural coordination patterns, thereby improving transparency and user comfort. In rehabilitation, identifying how synergy patterns adapt to reduced redundancy can inform targeted interventions that facilitate motor recovery by reinforcing these

natural coordination tendencies, ultimately enhancing functional movement outcomes.

This chapter starts with a literature review that describes the current redundancy resolution and synergy pattern at the joint level. Then, the research plan including the method, data collection, and post processing is displayed.

3.2 Literature Review

3.2.1 Redundancy Resolution

The human arm has seven degrees of freedom (DoFs), provided by the shoulder, elbow, and wrist joints, as shown in Figure 3.1. However, only six degrees of freedom are necessary to position the wrist and orient the palm [51]. The additional degree of freedom enables multiple configurations to achieve the same task. Although inverse kinematics solutions are not unique mathematically [52,53], motor control offers a distinct method for addressing arm redundancy as it moves through space. Resolving this redundancy is crucial for ensuring safe and effective interactions between humans and wearable robots [54]. For seamless integration, the inverse kinematics solution that addresses the redundancy in the human-wearable robot system must be consistent [55,56].

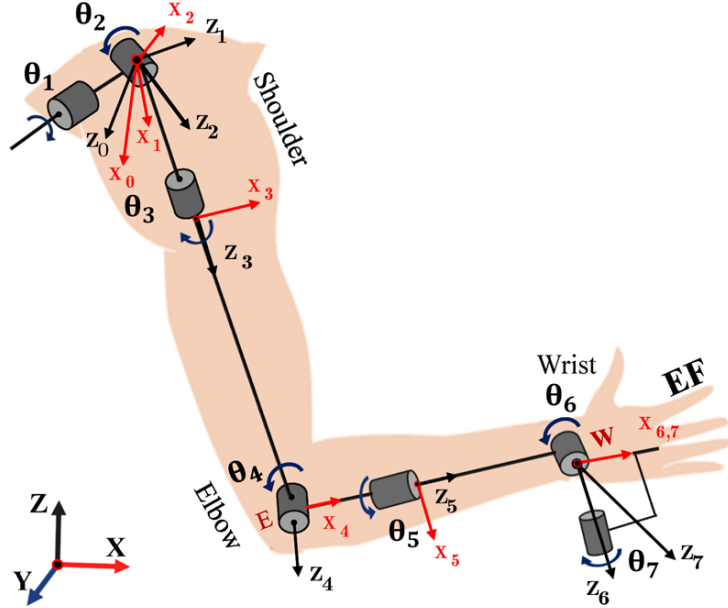


Figure 3.1: Arm model with shoulder adduction/abduction (θ_1), flexion/extansion (θ_2), and internal/external rotations (θ_3); elbow flexion/extansion (θ_4); and wrist supination/pronation (θ_5), radial/ulnar deviation (θ_6), and flexion/extansion (θ_7) [57].

A range of criteria and constraints has been proposed for arm motion formation and redundancy resolution, including the minimum-hand-jerk criterion [58], the minimum-torque

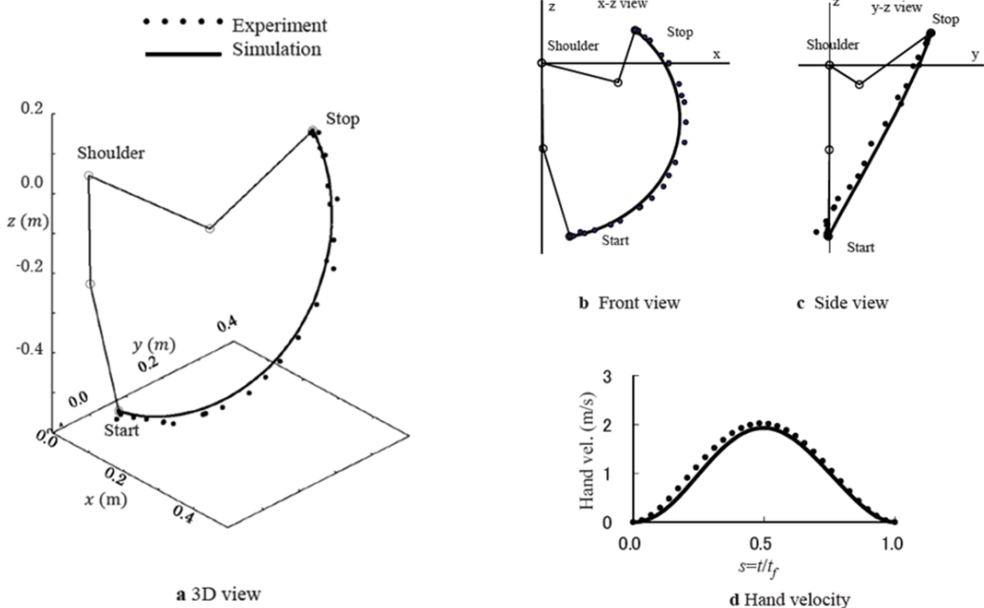


Figure 3.2: Trajectories generated by minimum-angular jerk with time adjustment [42].

change criterion [59], the minimum-variance criterion [60], and the minimum-work done criterion [61]. These criteria have been demonstrated to generate natural hand or joint trajectories. However, they primarily addresses motion within vertical or horizontal planes with two degrees of freedom. The application of these criteria to redundancy resolution in more complex scenarios has been rarely explored. In contrast, the minimum-angular-jerk criterion has been shown to closely replicate human arm motion, even in cases involving multiple joints and redundancy [44]. In [62], it is suggested that the hand trajectory becomes straighter when there is a delay in the onset of motion across multiple joints. Building on this, Tadashi et al. [42, 43] apply the minimum angular jerk criterion with time adjustment for the elbow to generate human-like arm trajectories. The delay in elbow motion is calculated by ensuring the hand's speed profile remains symmetric. This method achieves high accuracy for both long-distance and short-distance trajectories involving redundancy in three-dimensional space, as illustrated in Figure 3.2. However, this method breaks down whenever a substantial amount of joint reversal is required. Artemiadis et al. [63] have advanced the field by investigating joint dependencies through a Bayesian network. Their approach involves deriving an inverse kinematics solution based on an objective function constructed from these dependency relationships. Asfour et al. [53] employ a sensorimotor transformation model to map the wrist pose on a natural arm using a set of parameters related to upper arm elevation, the forearm elevation, the upper arm yaw and the forearm yaw. Kim et al. [55, 64] discover that when the elbow is flexed during reaching tasks, the palm points towards the head, which forms the basis for their approach to redundancy resolution. Li et al. [65] propose that the plane formed by the wrist, elbow, and shoulder rotates around a virtual axis for redundancy resolution during wrist movement from one position to another.

They find that the virtual axis obtained from their experiments is closely aligned with the direction of the equilibrium vector measured in microgravity conditions by NASA [66]. Shen *et al.* [12] introduce a new index for arm postural stability (APSI), revealing that the swivel angle, used in redundancy resolution, may serve as an indicator of arm postural stability and task difficulty. Furthermore, the APSI shows a strong linear correlation with the swivel angle under loading conditions. Kim *et al.* [67] combine the criterion of maximum joint angle availability with a viscoelastic model to predict redundancy resolution. They find that the average error between the estimated and measured swivel angles is lower compared to the errors associated with kinematically based redundancy resolution criteria.

Nonetheless, redundancy resolution may not be governed by a single criterion or constraint. Li *et al.* [68] evaluated five criteria: maximum motion efficiency towards a virtual target in the head [55], maintenance of the equilibrium posture based on the rotational axis method [65], minimum joint angle change, minimum kinetic energy change, and minimum work in joint space. They found that the combination of these criteria varies at different locations in the task space. Furthermore, the redundancy resolution predicted using the exponential method to synthesize these five criteria proves to be highly accurate, as shown in Figure 3.3. Kashi *et al.* [69] synthesize two criteria: minimum angular joint displacement (MAD) and maximum joint range availability (JRA) of the shoulder. They find that the contributions to the synthesized criterion are 70% from MAD and 30% from JRA. Most criteria do not account for wrist motion when determining redundancy resolution. However, as inferred from [61], the wrist is likely to have an effect. Therefore, Kim *et al.* [70] address redundancy resolution by combining the maximum manipulability criterion with the joint angle availability of the wrist. Their approach demonstrates a high correlation between the estimated and actual swivel angles. Zacharias et al. [71] develop a method for generating human-like configurations by utilizing the rapid upper limb assessment (RULA) to evaluate the stresses and strains on the musculoskeletal system. This is integrated with a capability map that quantifies the proximity of subregions to the dexterous workspace and the reachable orientations of the robot arm. The proposed approach enhances the selection of natural start and goal configurations for the robot arm, and improves the efficiency of path planning. Michael *et al.* [72] present an algorithm that produces human-like motion by optimizing it with respect to spatiotemporal correspondence (STC), which emulates the coordinated effects of human joints connected by muscles. The algorithm enhances the recognition accuracy of robot motions by producing human-like movement patterns. Additionally, variance is introduced to further refine the human-likeness of the motion, making the robot's actions less repetitive.

3.2.2 Synergistic Motion

The human musculoskeletal system is remarkably complex, encompassing numerous DoFs. However, research indicates that the number of DoFs directly controlled by the human nervous system is fewer than the total number determined by a purely mechanical count [73].

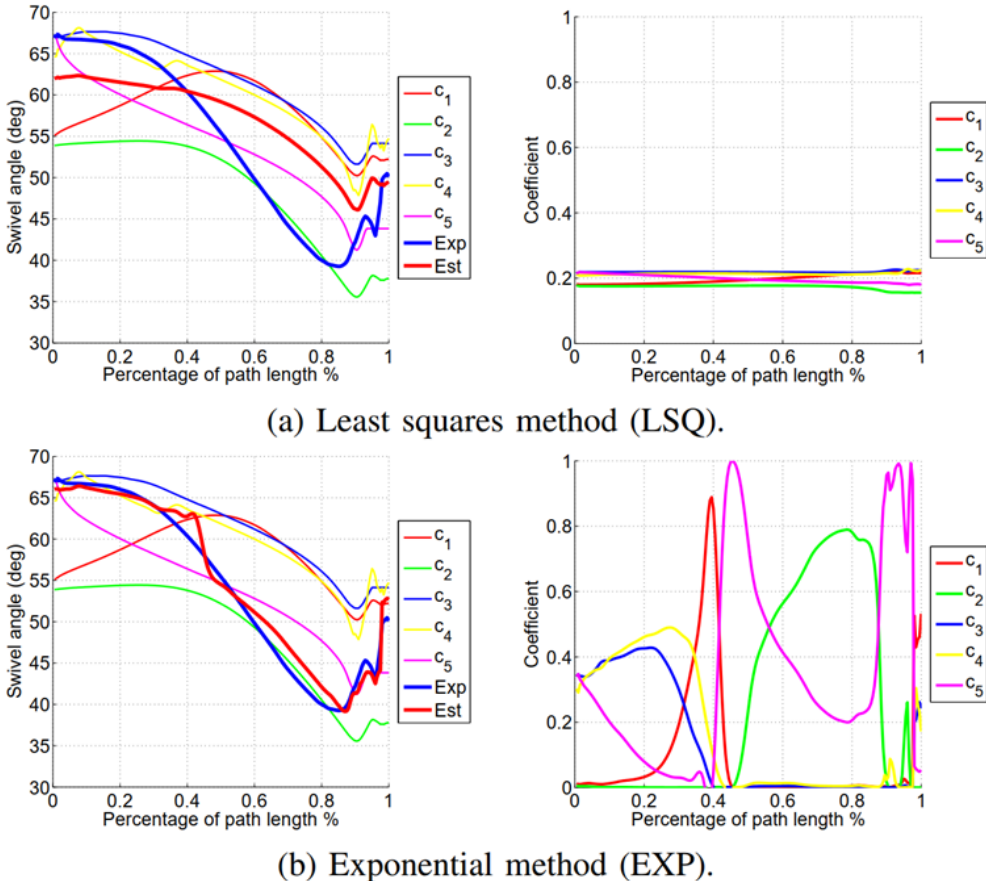


Figure 3.3: Estimated swivel angles based on the five criteria. (a) results obtained from the least square method (b) results obtained from the exponential method [68].

Research has extensively explored the concept of synergies across different levels, including muscular and kinematic levels, with a particular focus on the hand [74]. Synergies refer to the fundamental control patterns employed by the nervous system to coordinate the numerous DoFs and produce purposeful movements [75]. According to Latash *et al.* [76], synergies are characterized as a neural organization that produces task-specific covariation of elemental variables, ultimately aimed at achieving stable and effective movements. In their theory, unit elements can vary freely without individual control, a concept known as the Uncontrolled Manifold [76, 77].

At the muscular level, a common approach involves recording ElectroMyoGraphic (EMG) signals, followed by an identification of muscle co-activation patterns. D'Avella *et al.* [78] investigate the muscle activation patterns during frog kicking movements and identify that synergy recruitment is associated with movement kinematics. Their study also reveal that similar synergies can be extracted across different behavioral contexts. Castellini *et al.* [79] and Weiss *et al.* [80] both analyze grasping movements or posture using Principal Component

Analysis (PCA) of muscle activation data. Both studies find that the first few principal components of EMG signals account for a significant portion of the signal variance. Their findings collectively set a lower bound for the quantitative assessment of these patterns. It is also asserted in [79] that muscle synergies represent a physiologically valid model of grasping, effectively capturing the underlying muscle activation patterns associated with these movements. In the aspect of force generation, Valero-Cuevas [81] examines the muscle synergies of a single finger when producing forces in dorsal, distal, and palmar directions. The study finds that the generation of low and moderate forces is facilitated by appropriately scaling the magnitude of a coordination pattern that is capable of producing maximal force. Poston *et al.* [82] expand the scope of the research from single-finger to multi-finger analysis. Their findings indicate that the distribution of neural drive among various hand muscles remains constant regardless of the applied force. This pattern may be indicative of the anatomical structure or specific functional roles of different muscle groups in the hand. Maier *et al.* [83] investigate the synergies between muscle pairs in the hand and observe that, during the gripping process, the distribution of synergies in the amplitude domain of the EMG activity is similar across intrinsic muscles, extrinsic muscles, and their combinations. At the upper-limb level, D’Avella *et al.* [84] demonstrate that muscle synergies can effectively reconstruct movement patterns for various fast point-to-point tasks, regardless of load or forearm posture, and also for reversal and via-point movements. Their findings indicate that the intricate spatiotemporal dynamics of muscle patterns involved in reaching can be represented by a limited set of components. Similar outcomes have been documented in research concerning lower-limb dynamics [85]. For chronic stroke survivors, altered shoulder muscle synergies during 3-dimensional force matching are documented [86], and changes in these synergies due to robotic therapy are also reported [87]. Additionally, an impairment index based on movement complexity differences between affected and unaffected limbs, using the cumulative of variance from functional principal components, is proposed in [88].

At the kinematic level, joint positions are analyzed through PCA and Non-Negative Matrix Factorization, with a primary focus on synergies in the hand [75]. Averta *et al.* [89] demonstrate that the hand/object relative poses that optimize force distribution remain largely consistent as additional synergies are incorporated. Additionally, it is shown that the first seven principal components alone are sufficient for achieving force closure in all configurations where the full set of synergies is effective [89], and these components account for most of the observed variance in hand postures [90]. Furthermore, [91] indicates that tactile impairment has a minimal effect on the first two synergies during grasping, while changes due to the contact with the environment predominantly affect higher-order principal components. Furthermore, eigenpostures and their temporal evolutions are found to be similar across subjects and grasps [92], and the first two eigenpostures can account for most of the variance in hand shape [92–94]. The first principal component shows a pattern of finger extension transitioning to flexion, while the second principal component become significant primarily in the latter half of the reaching movement [95]. In [75], a repeated PCA (rPCA) method is introduced for analyzing arm movements of 30 different daily-living tasks, where PCA is applied iteratively at each time step. The findings indicate that, unlike

the hand, the first three synergy components capture the majority of the variance in arm motion, and the subspace they define remains relatively stable during pure motion phases as shown in Figure 3.4a. Furthermore, the influence of these three components diminishes when the arm interacts with the environment. The authors suggest that the first three synergies could be essential for shaping gross motor movements, while higher-order synergies could be more suited for fine-tuning the motion. The PCA analysis reveals the global static synergy components, with arm motion reflected by the first three components depicted in Figure 3.4b. The first component corresponds to extension and flexion of the arm in the sagittal plane. The second component relates to adjusting the hand's vertical position, while the third component involves modulating the elbow's swivel angle. Furthermore, according to [96], the smoothness of the relationship between the angular velocities of the shoulder and elbow decreases as the load on the hand increases. Additionally, this relationship exhibits distinct characteristics depending on the direction of the target being grasped.

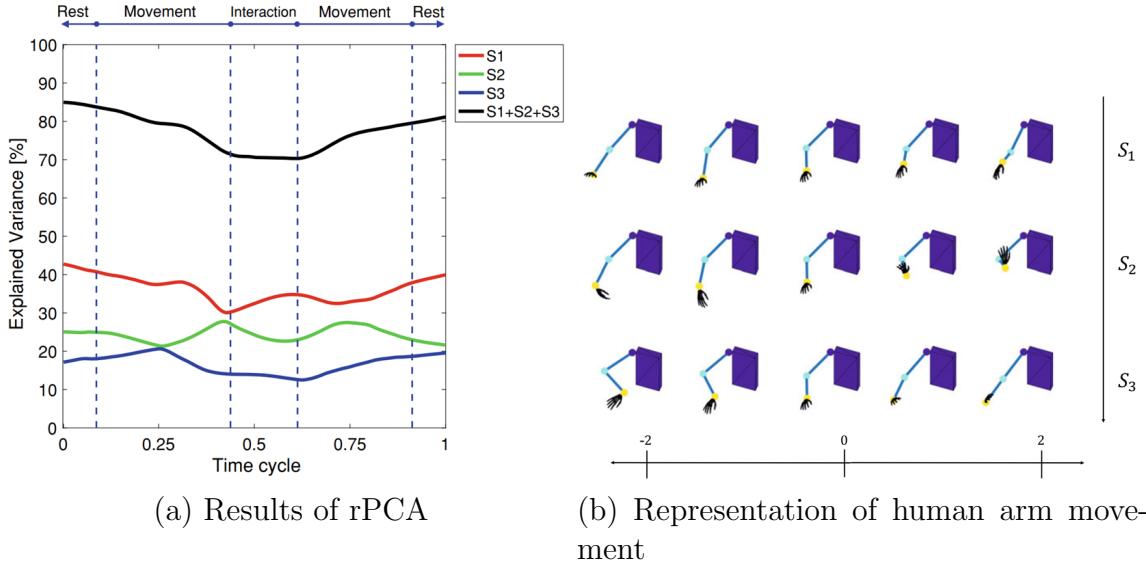


Figure 3.4: Synergy of arm movement [75].

For individuals who have suffered a stroke, the use of shoulder joints in coordination with the elbow and wrist may be more pronounced compared to healthy individuals [97]. Although individuals with mild-to-moderate hemiparesis exhibit variations in the synergy characteristics associated with specific joint coupling patterns, they still maintain the synergy feature related to error compensation [98].

3.3 Research Question

Previous research has explored the impact of external load, movement speed, object distance, object direction, and object orientation on the synergistic motion of the arm at the joint level.

However, the effect of the reduction of redundancy on this synergy remains inadequately understood. Therefore, a research question could be:

- How do humans form new movement synergies when some degrees of freedom in the arm are restricted?
- Do humans still follow the same redundancy resolution criteria when the available degrees of freedom are reduced?

Studying how synergy adapts to reduced degrees of freedom enhances our understanding of motor control and neural adaptation. It informs rehabilitation by optimizing training strategies for patients with movement impairments and improves exoskeleton design for more natural assistance. Additionally, insights from human synergy adaptation can enhance the motion planning of complex robotic systems.

3.4 Research Plan

The key research steps include:

3.4.1 Method

- Design devices that can stiffen one or multiple degrees of freedom of the wrist at a certain configuration since the effect of the wrist constraints are rarely investigated and the first four degrees of freedom are essential for reaching tasks;
- The constrained wrist/forearm configuration corresponds to the typical symptoms such as forearm pronation, wrist flexion, ulnar deviation.

3.4.2 Data Collection

- Assign 8 reaching targets in the workspace, as shown in Figure 3.5;
- Attach reflective markers on the arm, as shown in Figure 3.5;
- Collect kinematic data using motion capture system for the constrained condition;

3.4.3 Processing

- Conduct PCA on the data in the unconstrained condition to extract the mean motion synergy components;
- Use the mean synergy components to fit the motion in the unconstrained conditions;

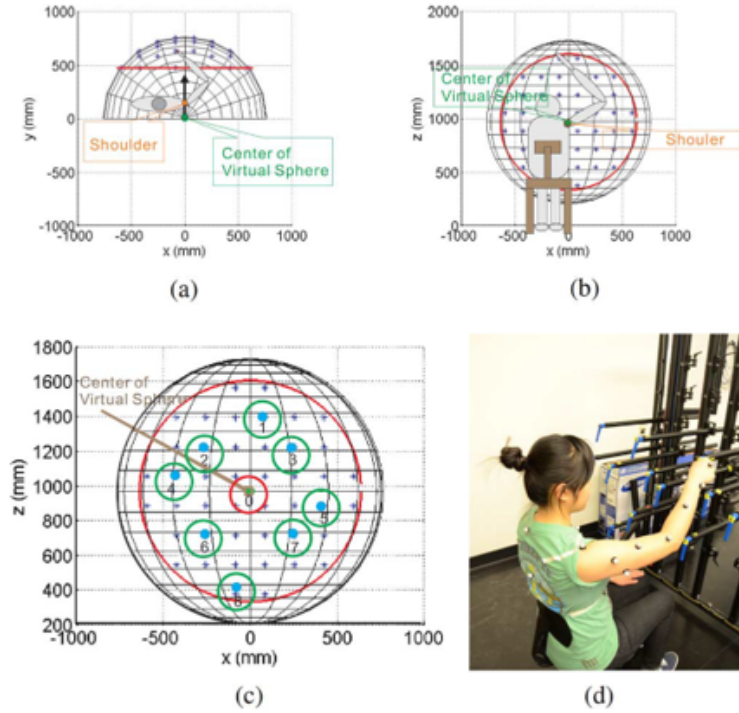


Figure 3.5: Reaching tasks [68]. (a) Top view (b) Front view (c) Task targets (d) Reflective markers on the arm.

- Compare the contribution of each synergy components between different constrained conditions;
- Get the redundancy resolution (swivel angle) based on the criteria of interest such as smoothness, minimum torque change, and joint range availability;
- Analyze the contribution of the criteria calculated based on the error between the actual swivel angle and the swivel angle obtained from the criteria with the decrease of redundancy.

CHAPTER 4

Augmentation of Physical Human-Exoskeleton Interaction Transparency

4.1 Introduction

The integration of robotics into human rehabilitation and assistance has gained significant momentum in recent years, with exoskeletons emerging as a promising solution to enhance mobility and facilitate recovery. A pivotal aspect of these systems is their ability to provide a high-quality free-motion experience, which is essential for fostering immersive human-robot interactions. The concept of transparency—where an exoskeleton does not impede or alter the user’s movements—plays a critical role in effective interaction. However, despite its theoretical appeal, achieving full transparency in practical applications remains largely unattainable due to the inherent weight of exoskeletons and the powerful actuators that can introduce significant resistance, inertia effects, and response delays [99], along with the complexities of human motion dynamics [100]. Consequently, research efforts are increasingly focused on enhancing mechanical designs and developing sophisticated control strategies that can better accommodate human variability.

Among these strategies, admittance control has been widely adopted to implement a transparent mode, primarily due to its intrinsic safety characteristics. By regulating the relationship between the force applied by the user and the resulting motion of the exoskeleton, admittance control ensures that the system responds in a stable and predictable manner, even under unexpected interactions. This is particularly important in scenarios where users may apply sudden or inconsistent forces—common in post-stroke rehabilitation or among users with impaired motor control. The ability to finely tune the virtual impedance allows the exoskeleton to yield appropriately to user intent, while preventing abrupt actuator reactions that could pose risks. Thus, admittance control serves as a critical safety mechanism, enabling a compliant interface that protects both the user and the robotic system during physical interaction.

Improving transparency not only enhances comfort and reduces physical strain but also strengthens the safety and effectiveness of human-robot interaction. A transparent system minimizes unintended resistance and enables users to move more freely and naturally, which is essential for re-engaging neuromuscular pathways and promoting long-term rehabilitation outcomes. Moreover, transparency fosters user trust, an important factor for sustained use of assistive technologies in daily life and therapy.

This chapter firstly reviews the prior methods, discusses the advantages and limitations of the methods, and describes the common measures of transparency. Then, the concept of the transparency balance is proposed and the research plans aiming to optimize the weighting and amplification of the force/torque sensor readings based on the newly proposed concept are displayed.

4.2 Literature Review

4.2.1 Transparency Improvement

Providing a high-quality free-motion experience is crucial for creating immersive human-robot interactions. However, exoskeletons face significant challenges in delivering free-motion rendering due to their relatively heavy weight and strong actuators [99]. Research presented in [101] indicates that the velocity and acceleration of human arm movements are clearly reduced when an exoskeleton is worn compared to when it is not worn. When an exoskeleton does not affect human movement, it is considered as transparent. This scenario remains largely theoretical, as fully realizing it in practice is nearly impossible due to the unpredictability of human motion [100]. Nonetheless, achieving near-perfect transparency is attainable by enhancing mechanical design in terms of transmission [102, 103] and human-exoskeleton physical interfaces [104–106], properly designing control structures [14, 99, 107–109], and enhancing sensor fusion systems [110–132].

The design of the controllers inherently results in different levels of transparency. In [107], three transparent controllers are evaluated: one that relies on exoskeleton dynamics identification, another on force feedback control, and a third that integrates both methods. For the controller based on the dynamic identification, the robot dynamics is built as

$$M(q)\ddot{q} + C(q, \dot{q}) + g(q) + \text{sign}(\dot{q})\mu_c + \mu_v\dot{q} = \tau_m \quad (4.1)$$

where q , \dot{q} , and \ddot{q} represent the joint position, velocity, and acceleration vectors, respectively, M is the inertia matrix, C is the vector of centrifugal and Coriolis terms, g is the gravity vector, μ_c and μ_v are the Coulomb and viscous friction coefficient vectors, and τ_m is the motor torque vector. The authors only identify the gravity effects since the gravity torques are predominant. Then, the open-loop compensation (OL) is achieved by a feedforward torque $\hat{\tau}_m$ as follows.

$$\hat{\tau}_m = g(q) \quad (4.2)$$

The force feedback control (CL) is expressed as

$$\tau_{TF}(t) = -\mathcal{K}_p \mathcal{L} f_e(t) - \mathcal{K}_i \int_{t_0}^t \mathcal{L} f_e(s) ds \quad (4.3)$$

where τ_{TF} is the joint torques, \mathcal{K}_p and \mathcal{K}_i are the proportional and integral control gains respectively, f_e is the normal force read from the force/torque sensors, \mathcal{L} relates the lever

arms used to convert sensor forces to torques, and t_0 and t are the initial time and current time respectively. The combination of this two controllers (OLCL) is illustrated in Figure 4.1.

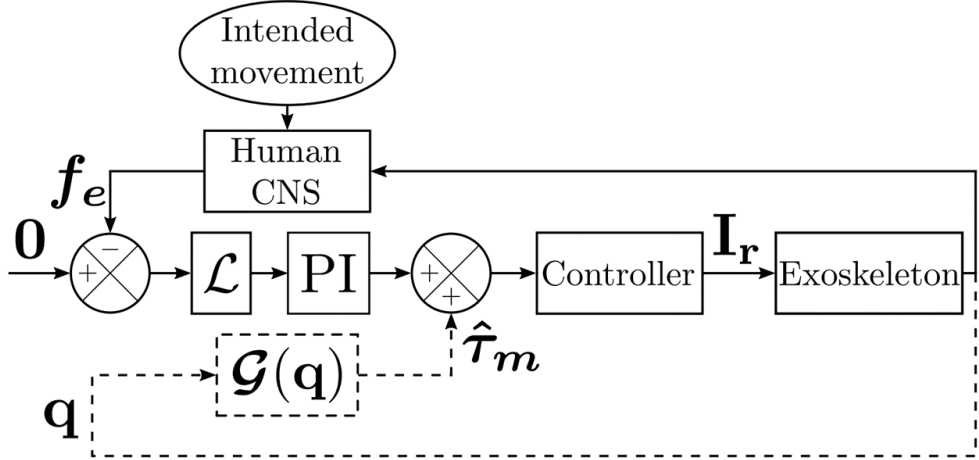


Figure 4.1: Complete controller: combination of the gravity compensation feedforward and force feedback [107].

After implementing reaching tasks in a parasagittal plane, it is found that the interaction forces recorded by the force/torque sensors for CL and OCOL are comparable and smaller than those of OL for the upper arm, while they are smallest for OLCL in the forearm. Conversely, OC exhibits the largest interaction forces over time for both the upper arm and forearm, as shown in Figure 4.2.

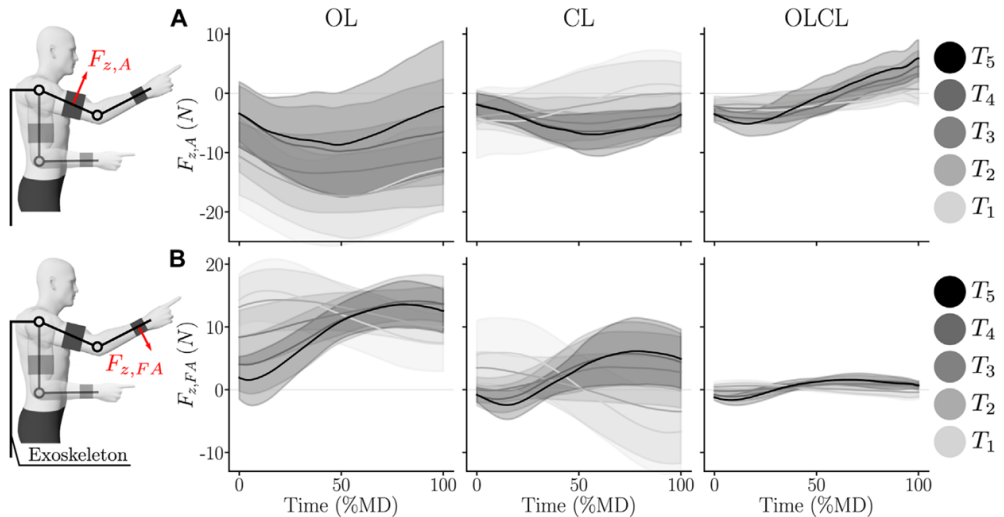
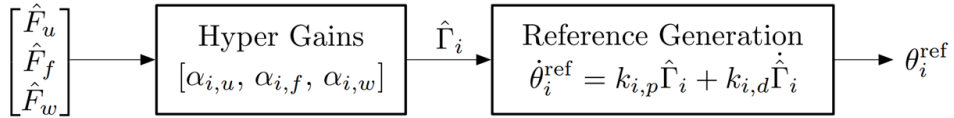


Figure 4.2: Interaction force on the upper arm and forearm [107].

Yang *et al.* [14] compare two admittance control schemes—one based on hyper parameters

and the other on a Kalman filter—as depicted in Figure 4.3. In the hyperparameter-based scheme, joint torques are derived through a weighted summation of partial torques mapped from sensor readings. Conversely, the Kalman filter-based scheme estimates joint torques under the assumption of Gaussian noise. The results indicate that the jerkiness of arm reaching movements is comparable between the two control schemes. However, the hyperparameter-based scheme generally exhibits lower power exchange, suggesting higher transparency, while the Kalman filter-based scheme provides more uniform transparency.

Scheme A :



Scheme B :

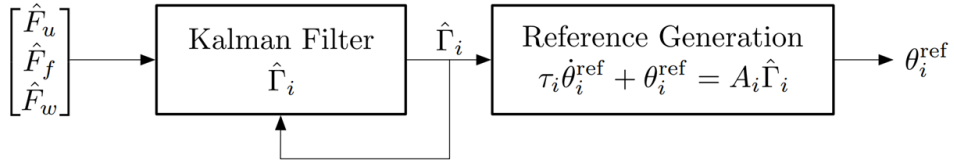


Figure 4.3: Admittance control schemes used in [14]. Scheme A: hyper parameter-based. Scheme B: Kalman filter-based.

Moreover, a new admittance controller based on the "head attraction" redundancy resolution [64] is developed in [108], as illustrated in Figure 4.4. The controller, with redundancy resolution support, demonstrates an 11.22% reduction in energy exchange compared to its counterpart without such support.

When humans control a robot using force sensors, the measured forces comprise not only the forces intentionally applied by the human but also the natural force feedback resulting from the interaction between the robot and the human arm during the robot's movement. To address this, an impedance compensator is added to the external force before it is processed by the admittance controller [109]. The compensator enhances transparency performance, as demonstrated by an increased magnitude and reduced phase lag in the system's frequency response when compared to a controller without the compensator.

Estimating the inertia term in exoskeleton dynamics poses a significant challenge, particularly when relying solely on encoder data, as discussed in [107]. This difficulty complicates dynamics identification and highlights the need for an enhanced sensor system. Research presented in [99] proposes addressing this issue by integrating joint encoder readings with inertia motion unit(IMU) data to estimate joint acceleration, thereby mitigating the impact of modeling errors on inverse dynamics. With enhanced acceleration estimation, a closed-loop acceleration controller can be incorporated into existing control schemes, also facilitating the design of more effective controller structures. The study evaluates the efficacy

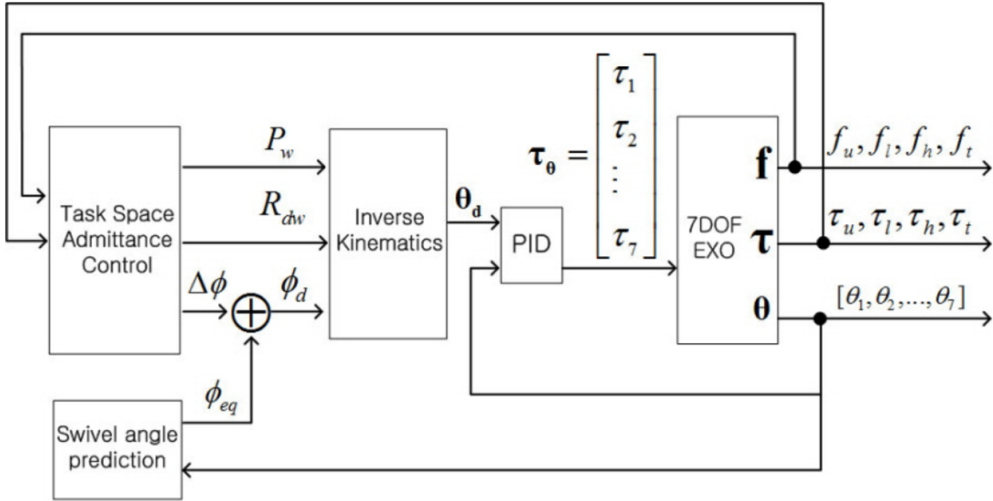


Figure 4.4: Admittance control based on redundancy resolution [108].

of a virtual mass controller with an acceleration closed-loop (VM+ATC) in comparison to a controller with only a feedforward compensation of dynamics. Results indicate that the VM+ATC controller significantly reduces both perceived inertia and joint torques induced by human-exoskeleton interactions.

Enhancing transparency in rehabilitation robotics can be achieved by capturing motion intention through sensor fusion. Sensor fusion can be categorized based on modalities and utilities. From a modality perspective, sensor fusion can be uni-modal or multi-modal. Uni-modal fusion involves integrating multiple sensors of the same type, whereas multi-modal fusion combines sensors of different types to comprehensively capture human motion intention. From a utility perspective, sensor fusion serves either classification or regression purposes. In classification, the fused sensor data predicts a high-level task that a low-level controller executes. In regression, the sensor fusion directly outputs the desired motion trajectory for the low-level controller to follow.

For uni-modal sensor fusion, various sensor types have been used to infer human motion intention, including electromyography (EMG) signals [110–114], brain activity measurements [115–118], and mechanical sensors such as force, torque, pressure sensors, and inertial measurement units (IMUs) [133–135]. Additionally, intraneuronal electrodes [119], mechanomyography (MMG) [120], and sonomyography (SMG) [121] have been employed to enhance motion intention detection.

Multi-modal sensor fusion can be categorized into four primary structures. The first is the single fusion algorithm, where features are extracted separately from each modality and then processed by a single sensor fusion algorithm [122–124]. The second is uni-modal switching, in which one modality is responsible for detecting transitions between operating modes and switching between different sensor fusion algorithms. Each of these algorithms, in turn, utilizes only the second modality as input [125–128]. The third structure is multi-modal

switching, which follows a similar principle but differs in that each sensor fusion algorithm integrates multiple modalities as inputs [129, 130]. Lastly, there is mixing, where multiple sensor fusion algorithms run in parallel, each incorporating one or more modalities. The outputs of these algorithms are then combined, with their respective weights determined by a specific modality [131, 132]. The choice of fusion structures depends on the nature of the operating modes. Uni-modal switching and multi-modal switching are most effective when operating modes are clearly distinguishable, such as discrete gait phases identified by foot switches. In contrast, mixing is preferable in scenarios where operating modes are more ambiguous due to sensor uncertainty or partial overlap.

In the field of wearable robotics, multi-modal sensor fusion has been extensively explored, particularly in combining electromyography (EMG) with mechanical sensors, where all four approaches have been implemented. Another prevalent combination involves eye tracking with either electroencephalography (EEG) or EMG, primarily applied to upper-limb control using either triggering or mixing methods. EEG can also be fused with EMG or intraneuronal muscle signals. While fusion involving more than two modalities is relatively rare, some studies have investigated such implementations.

4.2.2 Measures of Transparency

The measures of transparency are generally evaluated at three levels: muscular, kinematic, and dynamic. At the muscular level, authors in [100, 136] proposed a muscle activation-based (EMG-based) index T that links motor commands to the resulting acceleration of human motion, as shown below.

$$T = \frac{\ddot{q}_{max}}{A_{RMS}} \frac{A_{RMS,exo}}{\ddot{q}_{max,exo}} - 1 \quad (4.4)$$

where \ddot{q}_{max} and $\ddot{q}_{max,exo}$ are the maximum angular acceleration without and with wearing the exoskeleton respectively, and A_{RMS} and $A_{RMS,exo}$ are the root mean squared value of the activation of the agonist muscle without and with wearing the exoskeleton respectively. This index reflects the perceived effort of movement. However, it is better suited for horizontal planar motion due to the influence of gravity on the index. To assess transparency, muscle activation signals are compared across different controllers for the same tasks, as discussed in [107, 137]. Lower muscle activation suggests that less force is required to drive the limb, implying reduced resistance from the exoskeleton and, consequently, higher transparency—provided other variables are well controlled. Additionally, muscle synergies have been incorporated to analyze user transparency in [138]. For a transparent system, not only should muscle activation levels be low, but the muscle activation patterns should also remain consistent with those of the free motion. The similarity of these patterns can be quantified using the dot product between muscle patterns observed during free motion and those observed during motion assisted by exoskeletons. However, relying on individual muscle activation for transparency assessment remains challenging. EMG signals can be unstable during experiments due to factors such as potentiation or fatigue during repetitive trials.

Moreover, it is difficult to attribute transparency to individual muscles and calculate overall transparency, as different muscles exhibit distinct characteristics.

At kinematic level, transparency can also be assessed by comparing movement duration and maximum velocity between tasks performed with and without the exoskeleton [136]. These metrics can be obtained by fitting a bell-shaped velocity profile, as proposed in [58], which characterizes natural human motion. Other parameters, such as peak acceleration and trajectory curvature, are included to evaluate transparency in [107]. However, it is hard to quantify the transparency using multiple kinematic parameters. Besides, even though the kinematics are similar between two systems to be compared, the resistance from the dynamics or the muscle activities can be quite different. Furthermore, complicated motions can require more kinematic parameters to quantify the transparency. Therefore, the kinematics-based assessment should be implemented with the muscular or dynamics-based assessment.

At dynamic level, impedance-based transparency assessments, as described in [139], utilize interactive force and velocity data to determine how much interactive force contributes to human motion, as shown below.

$$IMP_{inertia} = \frac{\tau_i}{\ddot{q}_i} \quad IMP_{velocity} = \frac{\tau_i}{\dot{q}_i} \quad (4.5)$$

where $IMP_{inertia}$ and $IMP_{velocity}$ are the inertia and velocity impedance respectively, τ_i is the interactive torque on joint i , \ddot{q}_i is the angular acceleration of joint i , and \dot{q}_i is the angular acceleration of joint i . Similarly, average or peak interactive torque on joints over a specific duration is employed in [107, 137, 140–142]. Besides, a lower power exchange between the exoskeleton and the user also indicates higher transparency [14]. The power exchange PE is given by:

$$PE = \int_0^t \tau^T \dot{\theta}(s) ds \quad (4.6)$$

where τ is the interactive torque on the arm joints, and $\dot{\theta}$ is the angular velocity of the arm joints. Additionally, [99] uses the ratio of felt inertia to reflected inertia to assess wrench tracking accuracy, R , as shown below.

$$R = \frac{s_i J^T \tau}{s_i M \ddot{\theta}} \quad (4.7)$$

where s_i is a selection vector used to select the i^{th} element of the vector behind it, and M is the virtual mass matrix. A lower ratio corresponds to more accurate wrench tracking and, consequently, greater transparency. When relying solely on interactive force or the power exchange, it is essential to control other factors, such as kinematics, as they can influence force measurements even for identical tasks.

4.3 Research Question

To capture human motion intention and enhance transparency, various sensor fusion systems have been developed. In uni-modal sensor fusion, each sensor is typically responsible for a specific joint or task. However, in the case of EXO-UL8, multiple F/T sensors are employed, and their responsibilities overlap across joints. Consequently, the contribution of each sensor to different joints may vary depending on the state. Besides, for the current transparency evaluation, the overall transparency is typically investigated. However, whether the transparency is properly distributed across joints is not studied. Therefore, the research question could be:

- How can exoskeleton transparency including overall transparency and transparency balance, be enhanced through proper contribution of interdependent force/torque sensors for admittance controller?

4.4 Research Plan

The admittance control used in EXO-UL8 is based on F/T sensors. The sensors' readings go through a sensor fusion process to generate an equivalent torque τ_e which is used to reflect the human motion intention, as shown below.

$$\tau_e = \beta \sum_{i=u,f} \alpha_i \odot J_i^T W_i \quad (4.8)$$

where $\tau_e \in \mathbb{R}^4$ is the equivalent torque which accounts for the human motion intention, β is an amplification factor used to amplify the overall equivalent torque, $\alpha_i \in \mathbb{R}^4$ is the hyperparameter of the sensor fusion process which account for the contribution of the force sensor i on each joint, $J_i \in \mathbb{R}^{6 \times 4}$ is the jacobian of the force sensor i , and $W_i \in \mathbb{R}^6$ is the wrench readings from the force sensor i . The symbol \odot denotes the Hadamard product of two matrixes, and $i = u$, and f denotes the identification of the upper, lower, and wrist F/T sensor, respectively. In this study, first four degrees of freedom (3 shoulder DoFs and 1 elbow DoF) are considered. Hence, only the force/torque sensors on the upper arm and forearm are employed.

The contribution on each joint is normalized, as shown below, to make the calculation more stable and reliable and make the contribution of each sensor more understandable.

$$\sum_{i=u,f} \alpha_{i,j} = 1 \quad (4.9)$$

where $\alpha_{i,j}$ denotes the contribution of sensor i on the j^{th} joint.

For a perfect transparency, the interaction between the human and exoskeleton should be zero, implying the exoskeleton can perfectly predict the human motion intention and follow

the human motion exactly. In real scenario, it will never be achieved for the F/T sensor-based admittance controller since the sensors' readings are used to generate the motion. If the readings are always zero, the controller will think the human does not want to move in any direction. The transparency can be reflected by whether the motion intention is amplified properly and whether the contribution of the force/torque sensors is balanced. If the amplification of the motion intention signal is not proper, users will feel that the motion is too hard or too sensitive. Fortunately, the virtual mass and damping can be adjusted or an amplification factor can be multiplied with the equivalent torque to regulate the amplification of the motion intention signal. The unbalanced contribution of the sensors can make users feel hard to move some joints while too sensitive to move the others. In this study, the transparency includes both transparency balance (TB) and overall transparency of the whole system (OT).

Since the force/torque (F/T) sensor on the upper arm does not influence the elbow joint, the fourth element of α_u and α_f is set to 0 and 1, respectively, in accordance with equation (4.9). Given the first three elements of α_u , the corresponding first three elements of α_f can be determined using equation (4.9). In this study, these first three elements of α_u are optimized and represented as $\alpha_{u,p} \in \mathbb{R}^3$. Additionally, the amplification factor β is another parameter included in the optimization. Thus, the set of hyperparameters, denoted as p , is defined as:

$$p = [\alpha_{u,p}^T \quad \beta]^T \in \mathbb{R}^4$$

The optimization objective function $f(p_i)$ is a black-box function derived from experiments with a given input p_i and is expressed as:

$$f(p_i) = \gamma_{TB} TB(p_i) + \gamma_{OT} OT(p_i) + Error_i + \epsilon_i \quad (4.10)$$

where γ_{TB} and γ_{OT} are a weighting factor that balances the contribution of the two transparency indices, $Error_i$ is the distance between the stop point of the motion and the reaching target, and ϵ_i is the noise of the observation and follows a distribution of $\epsilon_i \sim \mathcal{N}(0, \sigma_i^2)$. The observation noise ϵ_i , which can mainly arise from human motion variability [143], may follow different distributions depending on the input, as motion intention is decoded differently with varying inputs. The optimization problem is formulated as:

$$\min_p f(p) \quad \text{s.t.} \quad p_i \in [p_{i,\min}, p_{i,\max}], \quad \dot{x} = f_{hybrid}(x) \quad (4.11)$$

where p_i denotes the i^{th} element of p , $p_{i,\min}$ and $p_{i,\max}$ represent its respective lower and upper bounds, and $\dot{x} = f_{hybrid}(x)$ is the dynamics of the human-exoskeleton hybrid system.

The key steps for the research question is to:

- Define the transparency balance and overall transparency;

- Design reaching targets in different regions of workspace using the first four DoFs;
- Instruct the subjects to reach the targets in their natural way within 1 second and 3 seconds. Each task is formed by the target and desired speed and repeated 10 times;
- Implement Bayesian optimization for the hyperparameter p for each task;
- Analyze the influence of regions of workspace on the optimal parameters p^* ;
- Analyze the influence of motion speed on the optimal parameters p^* ;

CHAPTER 5

Conclusion

This thesis addresses three key aspects of human–exoskeleton interaction: minimal-assistance control, redundancy resolution and synergistic motion under joint constraints, and transparency optimization in upper-limb exoskeletons.

In Chapter 2, we proposed an assist-as-needed strategy that minimizes external intervention by establishing an effort transmission cycle across joints. This method enables the exoskeleton to provide only the necessary level of support, thereby enhancing user engagement—which is critical for motor recovery.

Chapter 3 examined how the human arm resolves redundancy and how synergy patterns evolve as degrees of freedom are gradually reduced. The findings offer valuable insights into the adaptability of human motor control, provide guidance for stroke rehabilitation, and inform the design of robotic systems that emulate human-like redundancy resolution under constrained conditions.

In Chapter 4, we focused on optimizing exoskeleton transparency by introducing a novel metric, the transparency balance. The optimal hyperparameters for sensor fusion were identified using Bayesian optimization. We further analyzed how workspace region and movement speed affect these optimal parameters. This research contributes to building more immersive and natural interactions for rehabilitation and other applications of exoskeletons.

Together, these studies provide a comprehensive understanding of upper-limb motor behavior and offer practical methods for enhancing the effectiveness, comfort, and responsiveness of rehabilitation exoskeletons.

REFERENCES

- [1] Valery L Feigin, Michael Brainin, Bo Norrving, Sheila Martins, Ralph L Sacco, Werner Hacke, Marc Fisher, Jeyaraj Pandian, and Patrice Lindsay. World stroke organization (wso): Global stroke fact sheet 2022. *International Journal of Stroke*, 17(1):18–29, 2022. PMID: 34986727.
- [2] Johns Hopkins Medicine. Arm care after a stroke. <https://www.hopkinsmedicine.org/health/conditions-and-diseases/stroke/arm-care-after-a-stroke>. Accessed: 2024-06-26.
- [3] Judith D Schaechter. Motor rehabilitation and brain plasticity after hemiparetic stroke. *Progress in Neurobiology*, 73(1):61–72, 2004.
- [4] Wanjoo Park, Wookjin Jeong, Gyu-Hyun Kwon, Yun-Hee Kim, and Laehyun Kim. A rehabilitation device to improve the hand grasp function of stroke patients using a patient-driven approach. In *2013 IEEE 13th International Conference on Rehabilitation Robotics (ICORR)*, pages 1–4, 2013.
- [5] Beth E. Fisher and Katherine J. Sullivan. Activity-dependent factors affecting post-stroke functional outcomes. *Topics in Stroke Rehabilitation*, 8(3):31–44, 2001.
- [6] Robert W. Teasell, Norine C. Foley, Sanjit K. Bhogal, and Mark R. Speechley. An evidence-based review of stroke rehabilitation. *Topics in Stroke Rehabilitation*, 10(1):29–58, 2003.
- [7] Chang Ho Hwang, Jin Wan Seong, and Dae-Sik Son. Individual finger synchronized robot-assisted hand rehabilitation in subacute to chronic stroke: a prospective randomized clinical trial of efficacy. *Clinical Rehabilitation*, 26(8):696–704, 2012. PMID: 22261813.
- [8] Rachele Bertani, Corrado Melegari, Maria Cristina De Cola, Alessia Bramanti, Placido Bramanti, and Rocco Salvatore Calabró. Effects of robot-assisted upper limb rehabilitation in stroke patients: a systematic review with meta-analysis. *Neurological Sciences*, 38:1561–1569, 2017.
- [9] Albert C. Lo, Peter D. Guarino, Lorie G. Richards, Jodie K. Haselkorn, George F. Wittenberg, Daniel G. Federman, Robert J. Ringer, Todd H. Wagner, Hermano I. Krebs, Bruce T. Volpe, Christopher T. Bever, Dawn M. Bravata, Pamela W. Duncan, Barbara H. Corn, Alycia D. Maffucci, Stephen E. Nadeau, Susan S. Conroy, Janet M. Powell, Grant D. Huang, and Peter Peduzzi. Robot-assisted therapy for long-term upper-limb impairment after stroke. *New England Journal of Medicine*, 362(19):1772–1783, 2010. PMID: 20400552.

- [10] Janne M. Veerbeek, Anneli C. Langbroek-Amersfoort, Erwin E. H. van Wegen, Carel G. M. Meskers, and Gert Kwakkel. Effects of robot-assisted therapy for the upper limb after stroke: A systematic review and meta-analysis. *Neurorehabilitation and Neural Repair*, 31(2):107–121, 2017. PMID: 27597165.
- [11] Roberto Colombo, Fabrizio Pisano, Silvestro Micera, Alessandra Mazzone, Carmen Delconte, Maria Chiara Carrozza, Paolo Dario, and Giuseppe Minuco. Robotic techniques for upper limb evaluation and rehabilitation of stroke patients. *IEEE transactions on neural systems and rehabilitation engineering : a publication of the IEEE Engineering in Medicine and Biology Society*, 13:311–24, 09 2005.
- [12] Yang Shen, Brandon Po-Yun Hsiao, Ji Ma, and Jacob Rosen. Upper limb redundancy resolution under gravitational loading conditions: Arm postural stability index based on dynamic manipulability analysis. In *2017 IEEE-RAS 17th International Conference on Humanoid Robotics (Humanoids)*, pages 332–338, 2017.
- [13] Yang Shen, Ji Ma, Bruce Dobkin, and Jacob Rosen. Asymmetric dual arm approach for post stroke recovery of motor functions utilizing the exo-ul8 exoskeleton system: A pilot study. In *2018 40th Annual International Conference of the IEEE Engineering in Medicine and Biology Society (EMBC)*, volume 2018, pages 1701–1707, 07 2018.
- [14] Yang Shen, Jianwei Sun, Ji Ma, and Jacob Rosen. Admittance control scheme comparison of exo-ul8: A dual-arm exoskeleton robotic system. In *Conference: ICORR 2019 - 16th IEEE International Conference on Rehabilitation Robotics*, volume 2019, 05 2019.
- [15] José Leal-Naranjo, Marco Ceccarelli, and Christopher Torres San miguel. Mechanical design of a prosthetic human arm and its dynamic simulation. In *International Conference on Robotics in Alpe-Adria Danube Region*, volume 540, pages 482–490, 11 2017. ISBN 978-3-319-49057-1.
- [16] Salim S. Virani, Alvaro Alonso, Hugo J. Aparicio, Emelia J. Benjamin, Marcio S. Bittencourt, Clifton W. Callaway, April P. Carson, Alanna M. Chamberlain, Susan Cheng, Francesca N. Delling, Mitchell S.V. Elkind, Kelly R. Evenson, Jane F. Ferguson, Deepak K. Gupta, Sadiya S. Khan, Brett M. Kissela, Kristen L. Knutson, Chong D. Lee, Tené T. Lewis, Junxiu Liu, Matthew Shane Loop, Pamela L. Lutsey, Jun Ma, Jason Mackey, Seth S. Martin, David B. Matchar, Michael E. Mussolini, Sankar D. Navaneethan, Amanda Marma Perak, Gregory A. Roth, Zainab Samad, Gary M. Satou, Emily B. Schroeder, Svatı H. Shah, Christina M. Shay, Andrew Stokes, Lisa B. Van-Wagner, Nae-Yuh Wang, Connie W. Tsao, On behalf of the American Heart Association Council on Epidemiology, Prevention Statistics Committee, and Stroke Statistics Subcommittee. Heart disease and stroke statistics—2021 update. *Circulation*, 143(8):e254–e743, 2021.

- [17] Cerebrovascular disease or stroke. <https://www.cdc.gov/nchs/fastats/stroke.htm>. Accessed: 2024-10-03.
- [18] Ho Shing Lo and Sheng Quan Xie. Exoskeleton robots for upper-limb rehabilitation: State of the art and future prospects. *Medical Engineering & Physics*, 34(3):261–268, 2012.
- [19] Ali Utku Pehlivan, Fabrizio Sergi, and Marcia K. O’Malley. A subject-adaptive controller for wrist robotic rehabilitation. *IEEE/ASME Transactions on Mechatronics*, 20(3):1338–1350, 2015.
- [20] Mahdi Maaref, Alireza Rezazadeh, Kimia Shamaei, Renz Ocampo, and Tavakoli Mahdi. A bicycle cranking model for assist-as-needed robotic rehabilitation therapy using learning from demonstration. *IEEE Robotics and Automation Letters*, 1(2):653–660, 2016.
- [21] Lance Cai, Andy Fong, Chad Otoshi, Yongqiang Liang, Joel Burdick, Roland Roy, and Victor Edgerton. Implications of assist-as-needed robotic step training after a complete spinal cord injury on intrinsic strategies of motor learning. *The Journal of neuroscience : the official journal of the Society for Neuroscience*, 26:10564–8, 11 2006.
- [22] Ruihua Wei, Sivakumar Balasubramanian, Lihong Xu, and Jiping He. Adaptive iterative learning control design for rupert iv. In *2008 2nd IEEE RAS & EMBS International Conference on Biomedical Robotics and Biomechatronics*, pages 647–652, 2008.
- [23] Elena Vergaro, Maura Casadio, Valentina Squeri, Psiche Giannoni, Pietro Morasso, and Vittorio Sanguineti. Self-adaptive robot training of stroke survivors for continuous tracking movements. *Journal of NeuroEngineering and Rehabilitation*, 7(13), 2010.
- [24] Brandon Rohrer, Susan Fasoli, Hermano Igo Krebs, Richard Hughes, Bruce Volpe, Walter R. Frontera, Joel Stein, and Neville Hogan. Movement smoothness changes during stroke recovery. *Journal of Neuroscience*, 22(18):8297–8304, 2002.
- [25] Tommaso Proietti, Nathanaël Jarrassé, Agnès Roby-Brami, and Guillaume Morel. Adaptive control of a robotic exoskeleton for neurorehabilitation. In *2015 7th International IEEE/EMBS Conference on Neural Engineering (NER)*, pages 803–806, 2015.
- [26] Yida Guo, Yang Tian, Haoping Wang, and Shuaishuai Han. Adaptive hybrid-mode assist-as-needed control of upper limb exoskeleton for rehabilitation training. *Mechatronics*, 100:103188, 2024.
- [27] Ali Utku Pehlivan, Dylan P. Losey, and Marcia K. O’Malley. Minimal assist-as-needed controller for upper limb robotic rehabilitation. *IEEE Transactions on Robotics*, 32(1):113–124, 2016.

- [28] Eric T. Wolbrecht, Vicky Chan, David J. Reinkensmeyer, and James E. Bobrow. Optimizing compliant, model-based robotic assistance to promote neurorehabilitation. *IEEE Transactions on Neural Systems and Rehabilitation Engineering*, 16(3):286–297, 2008.
- [29] Marco Guidali, Philippe Schlink, Alexander Duschau-Wicke, and Robert Riener. Online learning and adaptation of patient support during adl training. In *2011 IEEE International Conference on Rehabilitation Robotics*, pages 1–6, 2011.
- [30] C. Bower, Hossein Taheri, and Eric Wolbrecht. Adaptive control with state-dependent modeling of patient impairment for robotic movement therapy. In *2013 IEEE 13th International Conference on Rehabilitation Robotics (ICORR)*, pages 1–6, 2013.
- [31] Ali Utku Pehlivian, Fabrizio Sergi, and Marcia K. O’Malley. A subject-adaptive controller for wrist robotic rehabilitation. *IEEE/ASME Transactions on Mechatronics*, 20(3):1338–1350, 2015.
- [32] Lincong Luo, Liang Peng, Chen Wang, and Zeng-Guang Hou. A greedy assist-as-needed controller for upper limb rehabilitation. *IEEE Transactions on Neural Networks and Learning Systems*, 30(11):3433–3443, 2019.
- [33] Alexandra Handley, Pippa Medcalf, Kate Hellier, and Dipankar Dutta. Movement disorders after stroke. *Age and Ageing*, 38(3):260–266, 03 2009.
- [34] Peter S. Lum, Carolyne Patten, Dhara Kothari, and Ruth Yap. Effects of velocity on maximal torque production in poststroke hemiparesis. *Muscle & Nerve*, 30(6):732–742, 2004.
- [35] Megan O. Conrad and Derek G. Kamper. Isokinetic strength and power deficits in the hand following stroke. *Clinical Neurophysiology*, 123(6):1200–1206, 2012.
- [36] Jie Chen and Ron J. Patton. *Robust Model-Based Fault Diagnosis for Dynamic Systems*, volume 3 of *The International Series on Asian Studies in Computer and Information Science*. Springer Publishing Company, Incorporated, 2012. ISBN 9780792384113.
- [37] Roberto Colombo. Chapter 8 - performance measures in robot assisted assessment of sensorimotor functions. In Roberto Colombo and Vittorio Sanguineti, editors, *Rehabilitation Robotics*, pages 101–115. Academic Press, 2018. ISBN 978-0-12-811995-2.
- [38] Li-Qun Zhang, Jongsang Son, Hyung-Soon Park, Sang Hoon Kang, Yunju Lee, and Yupeng Ren. Changes of shoulder, elbow, and wrist stiffness matrix post stroke. *IEEE Transactions on Neural Systems and Rehabilitation Engineering*, 25(7):844–851, 2017.
- [39] Sang Wook Lee, Kristen Triandafilou, Blair A. Lock, and Derek G. Kamper. Impairment in task-specific modulation of muscle coordination correlates with the severity of hand impairment following stroke. *PLOS ONE*, 8(7):1–18, 07 2013.

- [40] Mark L. Latash. *Progress in Motor Control: Structure-function relations in voluntary movements*. Progress in Motor Control. Human Kinetics, 1998. ISBN 9780736000277. LCCN 97044950.
- [41] Vincent C. K. Cheung, Andrea Turolla, Michela Agostini, Stefano Silvoni, Caoimhe Bennis, Patrick Kasi, Sabrina Paganoni, Paolo Bonato, and Emilio Bizzi. Muscle synergy patterns as physiological markers of motor cortical damage. *Proceedings of the National Academy of Sciences*, 109(36):14652–14656, 2012.
- [42] Tadashi Kashima, Keisuke Yanagihara, and Masao Iwaseya. Trajectory formation based on a human arm model with redundancy. In *IEEE International Conference on Systems, Man and Cybernetics*, pages 959–963, 10 2012. ISBN 978-1-4673-1713-9.
- [43] Tadashi Kashima and Katsuhiro Hori. Control of biomimetic robots based on analysis of human arm trajectories in 3d movements. *Artificial Life and Robotics*, 21, 12 2015.
- [44] Tadashi Kashima and Keita Sugawara. Experimental and theoretical analysis of human arm trajectories in 3d movements. *Artificial Life and Robotics*, 20, 07 2015.
- [45] Simon Goodman and Gerald Gottlieb. Analysis of kinematic invariances of multijoint reaching movement. *Biological cybernetics*, 73:311–22, 10 1995.
- [46] C Atkeson and J Hollerbach. Kinematic features of unrestrained vertical arm movements. *Journal of Neuroscience*, 5:2318–2330, 09 1985.
- [47] Lance Cai, Andy Fong, Yongqiang Liang, Joel Burdick, and Victor Edgerton. Assist-as-needed training paradigms for robotic rehabilitation of spinal cord injuries. In *IEEE International Conference on Robotics and Automation*, volume 2006, pages 3504 – 3511, 06 2006.
- [48] Jinsook Roh, William Z. Rymer, Eric J. Perreault, Seng Bum Yoo, and Randall F. Beer. Alterations in upper limb muscle synergy structure in chronic stroke survivors. *Journal of Neurophysiology*, 109(3):768–781, 2013. PMID: 23155178.
- [49] Thomas E. Twitchell. The restoration of motor function following hemiplegia in man. *Brain*, 74(4):443–480, 12 1951.
- [50] Jianwei Sun, Erik Harrison Kramer, and Jacob Rosen. A safety-focused admittance control approach for physical human-robot interaction with rigid multi-arm serial link exoskeletons. *IEEE/ASME Transactions on Mechatronics*, pages 1–12, 2024.
- [51] Joel C. Perry, Janet M. Powell, and Jacob Rosen. Isotropy of an upper limb exoskeleton and the kinematics and dynamics of the human arm. *Applied Bionics and Biomechanics*, 6(2):758631, 2009.

- [52] Deepak Tolani and Norman I. Badler. Real-time inverse kinematics of the human arm. *Presence: Teleoperators and Virtual Environments*, 5(4):393–401, 11 1996.
- [53] Tamim Asfour and Rüdiger Dillmann. Human-like motion of a humanoid robot arm based on a closed-form solution of the inverse kinematics problem. In *Proceedings 2003 IEEE/RSJ International Conference on Intelligent Robots and Systems (IROS 2003) (Cat. No.03CH37453)*, volume 2, pages 1407–1412 vol.2, 2003.
- [54] Jacob Rosen and Joel C. Perry. Upper limb powered exoskeleton. *International Journal of Humanoid Robotics*, 04(03):529–548, 2007.
- [55] Hyunchul Kim, Levi Makaio Miller, Aimen Al-Refai, Moshe Brand, and Jacob Rosen. Redundancy resolution of a human arm for controlling a seven dof wearable robotic system. In *2011 Annual International Conference of the IEEE Engineering in Medicine and Biology Society*, pages 3471–3474, 2011.
- [56] Joel C. Perry, Jacob Rosen, and Stephen Burns. Upper-limb powered exoskeleton design. *IEEE/ASME Transactions on Mechatronics*, 12(4):408–417, 2007.
- [57] Abubaker Ahmed, Hehua Ju, Yang Yang, and Hao Xu. An improved unit quaternion for attitude alignment and inverse kinematic solution of the robot arm wrist. *Machines*, 11(7), 2023.
- [58] Tamar Flash and Neville Hogan. The coordination of arm movements: an experimentally confirmed mathematical model. *Journal of Neuroscience*, 5(7):1688–1703, 1985.
- [59] Yoji Uno, Mitsuo Kawato, and R. Suzuki. Formation and control of optimal trajectory in human multijoint arm movement. minimum torque-change model. *Biol. Cybern.*, 61: 89–101, 1989.
- [60] Chris M. Harris and Daniel M. Wolpert. Signal-dependent noise determines motor planning. *Nature*, 394:780–784, 1998.
- [61] Tao Kang, Stephen H. Tillery, and Jiping He. Determining natural arm configuration along reaching trajectory. In *Proceedings of the 25th Annual International Conference of the IEEE Engineering in Medicine and Biology Society (IEEE Cat. No.03CH37439)*, volume 2, pages 1444–1447 Vol.2, 2003.
- [62] J Hollerbach and C Atkeson. Deducing planning variables from experimental arm trajectories: Pitfalls and possibilities. *Biological cybernetics*, 56:279–92, 02 1987.
- [63] Panagiotis K. Artermiadis, Pantelis T. Katsiaris, and Kostas J. Kyriakopoulos. A biomimetic approach to inverse kinematics for a redundant robot arm. *Auton Robot*, 29:293–308, 2010.

- [64] Hyunchul Kim, Levi Makaio Miller, Nancy Byl, Gary M. Abrams, and Jacob Rosen. Redundancy resolution of the human arm and an upper limb exoskeleton. *IEEE Transactions on Biomedical Engineering*, 59(6):1770–1779, 2012.
- [65] Zhi Li, Jay Ryan Roldan, Dejan Milutinović, and Jacob Rosen. The rotational axis approach for resolving the kinematic redundancy of the human arm in reaching movements. In *2013 35th Annual International Conference of the IEEE Engineering in Medicine and Biology Society (EMBC)*, pages 2507–2510, 2013.
- [66] William Dumouchel and Fanny O’Brien. *Integrating a robust option into a multiple regression computing environment*, page 41–48. Springer-Verlag, Berlin, Heidelberg, 1992. ISBN 0387976337.
- [67] Hyunchul Kim, Jay Ryan Roldan, Zhi Li, and Jacob Rosen. Viscoelastic model for redundancy resolution of the human arm via the swivel angle: Applications for upper limb exoskeleton control. In *2012 Annual International Conference of the IEEE Engineering in Medicine and Biology Society*, pages 6471–6474, 2012.
- [68] Zhi Li, Dejan Milutinovic, and Jacob Rosen. Spatial map of synthesized criteria for the redundancy resolution of human arm movements. *IEEE Transactions on Neural Systems and Rehabilitation Engineering*, 23(6):1020–1030, 2015.
- [69] Barak Kashi, Jacob Rosen, Moshe Brand, and Idit Avrahami. Synthesizing two criteria for redundancy resolution of human arm in point tasks. In *2011 Third World Congress on Nature and Biologically Inspired Computing*, pages 63–68, 2011.
- [70] Hyunchul Kim and Jacob Rosen. Predicting redundancy of a 7 dof upper limb exoskeleton toward improved transparency between human and robot. *Journal of Intelligent & Robotic Systems*, 80, 02 2015.
- [71] Franziska Zacharias, Christian Schlette, Florian Schmidt, Christoph Borst, J. Rossmann, and Gerd Hirzinger. Making planned paths look more human-like in humanoid robot manipulation planning. In *IEEE International Conference on Robotics and Automation*, 05 2011.
- [72] Michael Gielniak, Karen Liu, and Andrea Thomaz. Generating human-like motion for robots. *The International Journal of Robotics Research*, 32:1275–1301, 09 2013.
- [73] Karl Newell and David Vaillancourt. Dimensional change in motor learning. *Human movement science*, 20:695–715, 12 2001.
- [74] Marco Santello, Matteo Bianchi, M. Gabiccini, Emiliano Ricciardi, Gionata Salvietti, Domenico Prattichizzo, Marc Ernst, Alessandro Moscatelli, Henrik Jörntell, Astrid Kappers, Kostas Kyriakopoulos, Alin Schaeffer, Claudio Castellini, and Antonio Bicchi. Hand synergies: Integration of robotics and neuroscience for understanding the control of biological and artificial hands. *Physics of Life Reviews*, 17, 02 2016.

- [75] Giuseppe Averta. *Quantifying the Time-Invariance Properties of Upper Limb Synergies*, pages 47–62. Springer International Publishing, Cham, 2022. ISBN 978-3-030-92521-5.
- [76] Mark Latash, John Scholz, and Gregor Schöner. Toward a new theory of motor synergies. *Motor control*, 11:276–308, 08 2007.
- [77] John Scholz and Gregor Schöner. The uncontrolled manifold concept: identifying control variables for a functional task. *Experimental brain research. Experimentelle Hirnforschung. Expérimentation cérébrale*, 126:289–306, 07 1999.
- [78] Andrea D’Avella, Philippe Saltiel, and Emilio Bizzi. Combinations of muscle synergies in the construction of a natural motor behavior. *Nature neuroscience*, 6:300–8, 04 2003.
- [79] Claudio Castellini and Patrick van der Smagt. Evidence of muscle synergies during human grasping. *Biological cybernetics*, 107, 01 2013.
- [80] Erica Weiss and Martha Flanders. Muscular and postural synergies of the human hand. *Journal of neurophysiology*, 92:523–35, 08 2004.
- [81] Francisco Valero-Cuevas. Predictive modulation of muscle coordination pattern magnitude scales fingertip force magnitude over the voluntary range. *Journal of neurophysiology*, 83:1469–79, 03 2000.
- [82] Brach Poston, Alessander Danna-dos Santos, Mark Jesunathadas, Thomas Hamm, and Marco Santello. Force-independent distribution of correlated neural inputs to hand muscles during three-digit grasping. *Journal of neurophysiology*, 104:1141–54, 08 2010.
- [83] Marc Maier and Marie-Claude Hepp-Reymond. Emg activation patterns during force production in precision grip. ii. muscular synergies in the spatial and temporal domain. *Experimental brain research. Experimentelle Hirnforschung. Expérimentation cérébrale*, 103:123–36, 02 1995.
- [84] Andrea D’Avella and Francesco Lacquaniti. Control of reaching movements by muscle synergy combinations. *Frontiers in computational neuroscience*, 7:42, 04 2013.
- [85] Yuri Ivanenko, Richard Poppele, and Francesco Lacquaniti. Five basic muscle activation patterns account for muscle activity during human locomotion. *The Journal of physiology*, 556:267–82, 05 2004.
- [86] Jinsook Roh, William Rymer, Eric Perreault, Seng Bum Yoo, and Randall Beer. Alterations in upper limb muscle synergy structure in chronic stroke survivors. *Journal of neurophysiology*, 109, 11 2012.

- [87] Laura Dipietro, H Krebs, Susan Fasoli, Bruce Volpe, Christopher Bever, and Neville Hogan. Changing motor synergies in chronic stroke. *Journal of neurophysiology*, 98:757–68, 09 2007.
- [88] Anne Schwarz, Giuseppe Averta, Janne Veerbeek, Andreas Luft, Jeremia Held, Gae-tano Valenza, Antonio Bicchi, and Matteo Bianchi. A functional analysis-based approach to quantify upper limb impairment level in chronic stroke patients: a pilot study. In *Conference proceedings: Annual International Conference of the IEEE Engineering in Medicine and Biology Society. IEEE Engineering in Medicine and Biology Society. Conference*, volume 2019, pages 4198–4204, 07 2019.
- [89] Giuseppe Averta, Franco Angelini, Manuel Bonilla, Matteo Bianchi, and Antonio Bicchi. Incrementality and hierarchies in the enrollment of multiple synergies for grasp planning. *IEEE Robotics and Automation Letters*, PP, 04 2018.
- [90] Pramodsingh Thakur, Amy Bastian, and Steven Hsiao. Multidigit movement synergies of the human hand in an unconstrained haptic exploration task. *The Journal of neuroscience : the official journal of the Society for Neuroscience*, 28:1271–81, 02 2008.
- [91] Cosimo Della Santina, Matteo Bianchi, Giuseppe Averta, Simone Ciotti, Visar Arapi, Simone Fani, Edoardo Battaglia, Manuel Catalano, Marco Santello, and Antonio Bicchi. Postural hand synergies during environmental constraint exploitation. *Frontiers in Neurorobotics*, 11, 08 2017.
- [92] C.R. Mason, J.E. Gomez, and T.J. Ebner. Hand synergies during reach-to-grasp. *Journal of neurophysiology*, 86:2896–910, 01 2002.
- [93] Marco Santello, Martha Flanders, and John Soechting. Postural hand synergies for tool use. *The Journal of neuroscience : the official journal of the Society for Neuroscience*, 18:10105–15, 12 1998.
- [94] Marco Santello, Martha Flanders, and John Soechting. Patterns of hand motion during grasping and the influence of sensory guidance. *The Journal of neuroscience : the official journal of the Society for Neuroscience*, 22:1426–35, 02 2002.
- [95] Marco Santello, Martha Flanders, and John Soechting. Patterns of hand motion during grasping and the influence of sensory guidance. *The Journal of neuroscience : the official journal of the Society for Neuroscience*, 22:1426–35, 02 2002.
- [96] Mirjana Popović, Dejan Popović, and Rajko Tomović. Control of arm movements: Reaching synergies for neuroprostheses with life-like control. *Journal of Automatic Control*, 12, 01 2002.

- [97] Omid Heidari, John Roylance, Alba Perez-Gracia, and Eydie Kendall. Quantification of upper-body synergies: A case comparison for stroke and non-stroke victims. In *Proceedings of the ASME 2016 International Design Engineering Technical Conferences & Computers and Information in Engineering Conference*, page V05AT07A032, 08 2016.
- [98] Darcy Reisman and John Scholz. Aspects of joint coordination are preserved during pointing in persons with post-stroke hemiparesis. *Brain: a journal of neurology*, 126: 2510–27, 12 2003.
- [99] Yves Zimmermann, Emek Barış Küçüktabak, Farbod Farshidian, Robert Riener, and Marco Hutter. Towards dynamic transparency: Robust interaction force tracking using multi-sensory control on an arm exoskeleton. In *2020 IEEE/RSJ International Conference on Intelligent Robots and Systems (IROS)*, pages 7417–7424, 2020.
- [100] Dorian Verdel, Simon Bastide, Olivier Bruneau, Bastien Berret, and Nicolas Vignais. Improving and quantifying the transparency of an upper-limb robotic exoskeleton with a force sensor and electromyographic measures. In *Conference: 46ème Congrès Société Biomécanique, Computer Methods in Biomechanics and Biomedical Engineering*, 10 2021.
- [101] Simon Bastide, Nicolas Vignais, Franck Geffard, and Bastien Berret. Interacting with a “transparent” upper-limb exoskeleton: A human motor control approach. In *Conference: 2018 IEEE/RSJ International Conference on Intelligent Robots and Systems (IROS)*, pages 4661–4666, 10 2018.
- [102] Ruwan Gopura, Sanjaya Bandara, Kazuo Kiguchi, and George K.I. Mann. Developments in hardware systems of active upper-limb exoskeleton robots: A review. *Robotics and Autonomous Systems*, 75, 10 2015.
- [103] Philippe Garrec. *Screw and Cable Actuators (SCS) and Their Applications to Force Feedback Teleoperation, Exoskeleton and Anthropomorphic Robotics*, pages 167–191. IntechOpen, 02 2010. ISBN 978-953-7619-78-7.
- [104] Randa Mallat, Mohamad Khalil, Gentiane Venture, Vincent Bonnet, and Samer Mohammed. Human-exoskeleton joint misalignment: A systematic review. In *2019 Fifth International Conference on Advances in Biomedical Engineering (ICABME)*, pages 1–4, 10 2019.
- [105] André Schiele and Frans van der Helm. Influence of attachment pressure and kinematic configuration on phri with wearable robots. *Applied Bionics and Biomechanics*, 6:157–173, 07 2009.
- [106] Dorian Verdel, Guillaume Sahm, Simon Bastide, Olivier Bruneau, Bastien Berret, and Nicolas Vignais. Influence of the physical interface on the quality of human-exoskeleton interaction. *IEEE Transactions on Human-Machine Systems*, PP:1–10, 01 2022.

- [107] Dorian Verdel, Anais Farr, Thibault Devienne, Nicolas Vignais, Bastien Berret, and Olivier Bruneau. Human movement modifications induced by different levels of transparency of an active upper limb exoskeleton. *Frontiers in Robotics and AI*, 11:1308958, 01 2024.
- [108] Hyunchul Kim, Levi Miller, Zhi Li, Jay Roldan, and Jacob Rosen. Admittance control of an upper limb exoskeleton - reduction of energy exchange. *Conference proceedings: Annual International Conference of the IEEE Engineering in Medicine and Biology Society. IEEE Engineering in Medicine and Biology Society. Conference*, 2012:6467–70, 08 2012.
- [109] Kyeong Lee, Seung Baek, Hyuk Lee, Hyouk Choi, Hyungpil Moon, and Ja Koo. Improving transparency in physical human-robot interaction using an impedance compensator. In *2017 IEEE/RSJ International Conference on Intelligent Robots and Systems (IROS)*, pages 3591–3596, 09 2017.
- [110] Tomohiro Hayashi, Hiroaki Kawamoto, and Yoshiyuki Sankai. Control method of robot suit hal working as operator’s muscle using biological and dynamical information. *2005 IEEE/RSJ International Conference on Intelligent Robots and Systems*, pages 3063–3068, 2005.
- [111] Tommaso Lenzi, Stefano Marco Maria De Rossi, Nicola Vitiello, and Maria Chiara Carrozza. Intention-based emg control for powered exoskeletons. *IEEE Transactions on Biomedical Engineering*, 59(8):2180–2190, 2012.
- [112] J. Rosen, M. Brand, M.B. Fuchs, and M. Arcan. A myosignal-based powered exoskeleton system. *IEEE Transactions on Systems, Man, and Cybernetics - Part A: Systems and Humans*, 31(3):210–222, 2001.
- [113] Ning Jiang, Ivan Vujaklija, Hubertus Rehbaum, Bernhard Graimann, and Dario Farina. Is accurate mapping of emg signals on kinematics needed for precise online myoelectric control? *IEEE transactions on neural systems and rehabilitation engineering : a publication of the IEEE Engineering in Medicine and Biology Society*, 22, 10 2013.
- [114] J. M. Hahne, H. Rehbaum, F. Biessmann, F. C. Meinecke, K.-R. Müller, N. Jiang, D. Farina, and L. C. Parra. Simultaneous and proportional control of 2d wrist movements with myoelectric signals. In *2012 IEEE International Workshop on Machine Learning for Signal Processing*, pages 1–6, 2012.
- [115] Rupert Ortner, Brendan Allison, Gerd Korisek, Herbert Gaggl, and Gert Pfurtscheller. An ssvep bci to control a hand orthosis for persons with tetraplegia. *IEEE transactions on neural systems and rehabilitation engineering : a publication of the IEEE Engineering in Medicine and Biology Society*, 19:1–5, 09 2010.

- [116] Yongwook Chae, Jaeseung Jeong, and Sungho Jo. Toward brain-actuated humanoid robots: Asynchronous direct control using an eeg-based bci. *IEEE Transactions on Robotics*, 28(5):1131–1144, 2012.
- [117] Zuoguan Wang, qiang ji, Kai J. Miller, and Gerwin Schalk. Prior knowledge improves decoding of finger flexion from electrocorticographic signals. *Frontiers in Neuroscience*, 5, 2011.
- [118] Yasuhiko Nakanishi, Takufumi Yanagisawa, Duk Shin, Ryohei Fukuma, Chao Chen, Hiroyuki Kambara, Natsue Yoshimura, Masayuki Hirata, Toshiki Yoshimine, and Yasuharu Koike. Prediction of three-dimensional arm trajectories based on ecog signals recorded from human sensorimotor cortex. *PLOS ONE*, 8(8):1–9, 08 2013.
- [119] Silvestro Micera, Luca Citi, Jacopo Rigosa, Jacopo Carpaneto, Stanisa Raspopovic, Giovanni Di Pino, Luca Rossini, Ken Yoshida, Luca Denaro, Paolo Dario, and Paolo Maria Rossini. Decoding information from neural signals recorded using intraneurial electrodes: Toward the development of a neurocontrolled hand prosthesis. *Proceedings of the IEEE*, 98(3):407–417, 2010.
- [120] Jorge Silva, Winfried Heim, and Tom Chau. A self-contained, mechanomyography-driven externally powered prosthesis. *Archives of Physical Medicine and Rehabilitation*, 86(10):2066–2070, 2005.
- [121] Xin Chen, Yong-Ping Zheng, Jing-Yi Guo, and Jun Shi. Sonomyography (smg) control for powered prosthetic hand: A study with normal subjects. *Ultrasound in Medicine & Biology*, 36(7):1076–1088, 2010.
- [122] Kazuo Kiguchi, Shingo Kariya, Kimitsuna Watanabe, Kiyotaka Izumi, and Toshio Fukuda. An exoskeletal robot for human elbow motion support - sensor fusion, adaptation, and control. *IEEE transactions on systems, man, and cybernetics. Part B, Cybernetics : a publication of the IEEE Systems, Man, and Cybernetics Society*, 31:353–61, 02 2001.
- [123] Arjan Gijsberts and Barbara Caputo. Exploiting accelerometers to improve movement classification for prosthetics. In *2013 IEEE 13th International Conference on Rehabilitation Robotics (ICORR)*, pages 1–5, 2013.
- [124] Anders Fougnier, Erik Scheme, Adrian Chan, Kevin Englehart, and Øyvind Stavdahl. A multi-modal approach for hand motion classification using surface emg and accelerometers. *Conference proceedings : ... Annual International Conference of the IEEE Engineering in Medicine and Biology Society. IEEE Engineering in Medicine and Biology Society. Conference*, 2011:4247–50, 08 2011.
- [125] Yanjuan Geng, Ping Zhou, and Patrick Li. Toward attenuating the impact of arm positions on electromyography pattern-recognition based motion classification in transradial amputees. *Journal of neuroengineering and rehabilitation*, 9:74, 10 2012.

- [126] Anders Fougner, Erik Scheme, Adrian Chan, Kevin Englehart, and Øyvind Stavdahl. Resolving the limb position effect in myoelectric pattern recognition. *IEEE transactions on neural systems and rehabilitation engineering : a publication of the IEEE Engineering in Medicine and Biology Society*, 19:644–51, 08 2011.
- [127] Fan Zhang, Susan D’Andrea, Michael Nunnery, Steven Kay, and He Huang. Towards design of a stumble detection system for artificial legs. *IEEE transactions on neural systems and rehabilitation engineering : a publication of the IEEE Engineering in Medicine and Biology Society*, 19:567–77, 08 2011.
- [128] Samuel Au, Max Berniker, and Hugh Herr. Powered ankle-foot prosthesis to assist level-ground and stair-descent gaits. *Neural networks : the official journal of the International Neural Network Society*, 21:654–66, 06 2008.
- [129] Fan Zhang and H. Huang. Decoding movement intent of patient with multiple sclerosis for the powered lower extremity exoskeleton. *2013 35th Annual International Conference of the IEEE Engineering in Medicine and Biology Society (EMBC)*, pages 4957–4960, 2013.
- [130] Lin Du, Fan Zhang, Ming Liu, and He Huang. Toward design of an environment-aware adaptive locomotion-mode-recognition system. *IEEE Transactions on Biomedical Engineering*, 59(10):2716–2725, 2012.
- [131] Jia-Liang Ren, Ya-Hui Chien, En-Yu Chia, Li-Chen Fu, and Jin-Shin Lai. Deep learning based motion prediction for exoskeleton robot control in upper limb rehabilitation. In *IEEE International Conference on Robotics and Automation (ICRA)*, pages 5076–5082, 05 2019.
- [132] Anirban Dutta, Konrad Kording, Eric Perreault, and Levi Hargrove. Sensor-fault tolerant control of a powered lower limb prosthesis by mixing mode-specific adaptive kalman filters. *Conference proceedings : ... Annual International Conference of the IEEE Engineering in Medicine and Biology Society. IEEE Engineering in Medicine and Biology Society. Conference*, 2011:3696–9, 08 2011.
- [133] Marco Guidali, Urs Keller, Verena Klamroth-Marganska, Tobias Nef, and Robert Riener. Estimating the patient’s contribution during robot-assisted therapy. *Journal of rehabilitation research and development*, 50:379–94, 06 2013.
- [134] Stefano Marco Maria De Rossi, Nicola Vitiello, Tommaso Lenzi, Renaud Ronsse, Bram Koopman, Alessandro Persichetti, Fabrizio Vecchi, A.J. Ijspeert, Herman Kooij, and Maria Chiara Carrozza. Sensing pressure distribution on a lower-limb exoskeleton physical human-machine interface. *Sensors*, 11:207–27, 01 2011.
- [135] Cleiton Caltran and Adriano A. G. Siqueira. Sensor fusion applied to position estimation and gait identification of an ankle-foot orthosis. In *ISSNIP Biosignals and Biorobotics Conference 2011*, pages 1–6, 2011.

- [136] Dorian Verdel, Simon Bastide, Nicolas Vignais, Olivier Bruneau, and Bastien Berret. An identification-based method improving the transparency of a robotic upper limb exoskeleton. *Robotica*, 39(9):1711–1728, 2021.
- [137] Emek Barış Küçüktabak, Yue Wen, Sangjoon J. Kim, Matthew R. Short, Daniel Ludvig, Levi Hargrove, Eric J. Perreault, Kevin M. Lynch, and José L. Pons. Haptic transparency and interaction force control for a lower limb exoskeleton. *IEEE Transactions on Robotics*, 40:1842–1859, 2024.
- [138] Andrea Chiavenna, Alessandro Scano, Matteo Malosio, Lorenzo Molinari Tosatti, and Franco Molteni. Assessing user transparency with muscle synergies during exoskeleton-assisted movements: A pilot study on the lightarm device for neurorehabilitation. *Applied Bionics and Biomechanics*, 2018(1):7647562, 2018.
- [139] Xing Chen, Yan Zeng, and Yuehong Yin. Improving the transparency of an exoskeleton knee joint based on the understanding of motor intent using energy kernel method of emg. *IEEE Transactions on Neural Systems and Rehabilitation Engineering*, 25(6):577–588, 2017.
- [140] Alexandre Oliveira Souza, Jordane Grenier, François Charpillet, Serena Ivaldi, and Pauline Maurice. Enhancing exoskeleton transparency with motion prediction: An experimental study. In *2024 IEEE-RAS 23rd International Conference on Humanoid Robots (Humanoids)*, pages 744–751, 2024.
- [141] Yuepeng Qian, Shuaishuai Han, Yining Wang, Haoyong Yu, and Chenglong Fu. Toward improving actuation transparency and safety of a hip exoskeleton with a novel nonlinear series elastic actuator. *IEEE/ASME Transactions on Mechatronics*, 28(1):417–428, 2023.
- [142] Felix M. Escalante, Leonardo F. dos Santos, Yecid Moreno, Adriano A. G. Siqueira, Marco H. Terra, and Thiago Boaventura. Markovian transparency control of an exoskeleton robot. *IEEE Robotics and Automation Letters*, 8(2):544–551, 2023.
- [143] Mark L. Latash. Front matter. In *Fundamentals of Motor Control*, page iii. Academic Press, San Diego, 2012. ISBN 978-0-12-415956-3.

APPENDIX A

Gantt Chart

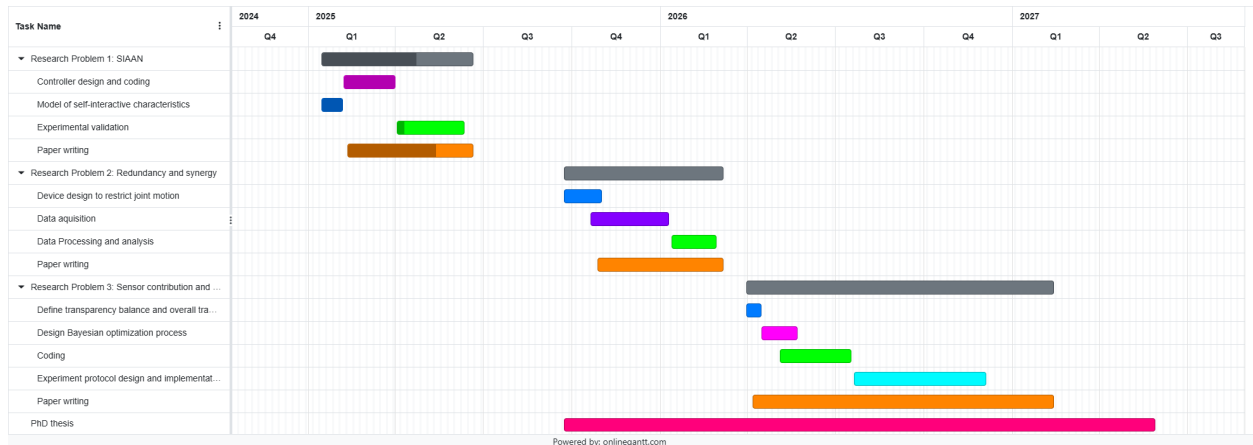


Figure A.1: Gantt chart for PhD research